Numerical studies on real time evolution in quantum systems - Quantum decoherence and the beginning of the universe

Yamamori Naoyuki

Doctor of Philosophy

Department of Particle and Nuclear Physics
School of High Energy Accelerator Science

The Graduate University for Advanced Studies, SOKENDAI

March 2026

Abstract

Real-time path integrals provide a natural formulation of quantum dynamics also in situations where a Hamiltonian description is unavailable or impractical, but their direct evaluation is obstructed by severe phase cancellation from the oscillatory weight. A guiding theme of this thesis is that, after complexifying the integration variables, real-time path integrals are naturally organized by complex saddle points. In favorable cases the original contour can be replaced by steepest-descent manifolds (Lefschetz thimbles) attached to the relevant saddles, providing a controlled saddle-based description of real-time observables.

In Part I, we study quantum decoherence in a closed-system real-time path-integral formulation: the total system (subsystem plus environment) evolves unitarily, and the environment is traced out only at the final time to obtain the reduced density matrix. For the Caldeira–Leggett model with Gaussian initial conditions, the discretized effective action becomes a quadratic form, so that the reduced density matrix is characterized by a complex saddle point and the thimble integral reduces to a finite-dimensional Gaussian integral. The complex saddle is obtained by solving a large but sparse linear system, allowing an exact evaluation of the reduced density matrix without relying on the usual master-equation approximations. We then extend this methodology to a three-dimensional cubic lattice toy model by separating center-of-mass and relative coordinates, treating the center-of-mass mode as the subsystem and the relative modes as an effective environment. This enables controlled numerical studies of how the suppression of off-diagonal matrix elements depends on the coupling, inverse temperature, and system size, and allows us to extract the early-time scaling behavior of decoherence diagnostics from the complex-saddle evaluation.

In Part II, we investigate spacetime dynamics in the Lorentzian IKKT matrix model. To define a Lorentzian formulation that is not continuously connected to the Euclidean model by the standard contour deformation, we include a Lorentz invariant mass term with coefficient γ, for which the classical equations admit real, smooth, expanding solutions when $\gamma > 0$. Since the Lorentz group is noncompact, the path integral can contain a divergent volume from the boost directions; we remove this volume nonperturbatively by implementing a boost "gauge-fixing" that selects the frame minimizing $\mathrm{tr}(A_0)^2$, leading to the condition $\mathrm{tr}(A_0 A_i) = 0$ with the associated Faddeev–Popov determinant. We then apply the complex Langevin method to the resulting complex-weight matrix integral. Time and spatial observables are defined from matrix configurations, with holomorphic time ordering implemented by auxiliary variables, and spatial structure characterized through block observables such as the extent $R^2(t)$ and the moment-of-inertia tensor. In the bosonic model we find approximately real time and no indication of spontaneous breaking of the spatial symmetry in the

parameter range studied. Including fermions, we control the singular-drift problem induced by the Pfaffian by introducing a fermionic mass regulator m_{f} and an anisotropic mass deformation, which enhances fermionic effects while maintaining numerical stability. In this setup we observe a real, expanding spatial extent and a dynamical dominance of three spatial directions at late times, consistent with a $(3+1)$-dimensional expanding spacetime. We finally discuss the intended limiting procedure—taking the large-N limit first and then approaching the undeformed theory—and comment on future directions, including a comparison with partially supersymmetric deformations that preserve 16 supercharges.

Contents

1 Introduction

Real-time dynamics in quantum systems is typically formulated in two complementary frameworks: the Schrödinger picture and the Feynman path integral. In many-body quantum mechanics, a direct Schrödinger-picture simulation requires resources that grow rapidly with the number of degrees of freedom, making systematic scaling studies difficult. By contrast, the path integral reorganizes real-time dynamics into an oscillatory integral, which provides a natural starting point also in settings where a Hamiltonian description is unavailable or impractical.

A central obstacle in real time is the severe phase cancellation caused by the oscillatory weight. The guiding idea of this thesis is that real-time path integrals are naturally characterized by complex saddle points. After complexifying the integration variables, the original contour can be deformed into steepest-descent manifolds (Lefschetz thimbles) attached to the relevant saddles. This viewpoint organizes the dominant contributions by complex saddles and their quadratic fluctuations, rather than by sampling on the original real contour.

Against this background, the present work carries out numerical studies of real-time dynamics within the path-integral formalism in two complementary settings: quantum decoherence in many-body quantum mechanics and spacetime dynamics in the Lorentzian IKKT matrix model. In both cases, complexification plays a structural role: in Part I it makes the complex-saddle description of the reduced density matrix explicit, while in Part II it underlies the complex Langevin method applied to the Lorentzian matrix integral.

Part I: Quantum decoherence from complex saddles.

Part I studies quantum decoherence from a complex-saddle representation of the reduced density matrix. Quantum decoherence denotes the environment-induced suppression of off-diagonal elements of a reduced density matrix, i.e., the decay of interference, and it provides a quantitative viewpoint on the quantum-to-classical transition. As a standard benchmark, we first consider the Caldeira–Leggett (CL) model, in which a distinguished degree of freedom couples linearly to a bath of harmonic oscillators. In the conventional continuum treatment, one derives a master equation for the reduced density matrix under the Ohmic, high-temperature, and Markov assumptions. While this framework is powerful, its quantitative reliability can become subtle outside the regime where these assumptions are justified.

In this thesis we instead emphasize a closed-system real-time path-integral formulation: the total system (system plus environment) evolves unitarily, and the environment is traced out only at the final time to obtain the reduced density matrix. In this representation the

effective action is complex, and the reduced density matrix is characterized by a complex saddle point after discretization. In the CL model with Gaussian initial conditions, the discretized effective action becomes a quadratic form, so that the Lefschetz-thimble integral attached to the relevant saddle reduces to a finite-dimensional Gaussian integral. As a result, the reduced density matrix can be evaluated exactly by solving the linear system that determines the complex saddle, without relying on the master-equation approximation.

Motivated by mesoscopic interference experiments and by the broader question of how decoherence properties depend on system size, internal structure, and interaction strength, we then investigate a three-dimensional cubic lattice toy model intended to mimic a large molecule. Within a single closed model at the level of the action, we separate the degrees of freedom into center-of-mass (CM) and relative coordinates, treating the CM mode as the subsystem and the relative modes as an effective environment-like sector. This setup enables controlled numerical studies of how off-diagonal suppression depends on the coupling and the inverse temperature β, and allows us to extract the early-time scaling of the decoherence diagnostic from the complex-saddle evaluation of the reduced density matrix. In particular, comparing the molecular toy model with the CL benchmark, we find evidence that a composite system with many internal degrees of freedom can exhibit a qualitatively different dependence of decoherence on the microscopic coupling parameter from that of a point-like system coupled to an external bath.

Part II: Lorentzian IKKT matrix model and spacetime from matrices.

Superstring theory is a promising candidate for a unified theory that includes quantum gravity. At present, however, it is formulated only perturbatively, which leads to well-known difficulties. First, the theory admits an enormous number of vacua with different compactification patterns and distinct matter content. Within the perturbative regime these vacua are degenerate, and there is no principle to select a unique vacuum. Second, perturbation theory breaks down at the initial singularity of the universe. To address these issues, a nonperturbative formulation of superstring theory is required.

An attempt to resolve these difficulties via a nonperturbative formulation mirrors the success of lattice gauge theory in quantum chromodynamics. The IKKT matrix model has been proposed as a nonperturbative formulation of superstring theory. It is obtained by dimensional reduction of ten-dimensional $\mathcal{N} = 1$ $U(N)$ supersymmetric Yang–Mills theory to zero dimensions. The action is written in terms of $N \times N$ Hermitian matrices and possesses $\mathrm{SO}(9,1)$ Lorentz symmetry. Spacetime is not assumed *a priori* and is instead characterized from the matrix degrees of freedom.

Since the model does not come with a time coordinate *a priori*, investigations have proceeded within the path integral formulation, where one can define a notion of time and

spatial structure from matrix configurations. Recent studies based on analytic continuation by contour deformation have suggested that, within such prescriptions, the Lorentzian model can be continuously connected to the Euclidean one for holomorphic observables. A characteristic outcome is that the observables used to characterize the spatial extent can exhibit a fixed phase rotation of the Euclidean type, so that the extracted geometry is not purely real.

To pursue genuinely Lorentzian behavior, a Lorentz-invariant mass term with coefficient γ has been proposed. For $\gamma > 0$ the same contour deformation that connects the Lorentzian model to the Euclidean point is no longer admissible, and the classical equations of motion admit real, smooth, expanding solutions. A further obstacle in the Lorentzian formulation is the noncompactness of the Lorentz group, which can generate a divergent boost volume in the path integral. While a cutoff regularizes the integral, it explicitly breaks Lorentz symmetry and can leave residual artifacts. Following earlier work, we instead remove the boost volume nonperturbatively by implementing a "gauge-fixing" of Lorentz boosts in the path integral. We select a representative frame by minimizing $\mathrm{tr}(A_0^2)$, which leads to the condition $\mathrm{tr}(A_0 A_i) = 0$ $(i = 1, \ldots, 9)$, and derive the corresponding Faddeev–Popov determinant.

We then apply the complex Langevin method (CLM) to the resulting gauge-fixed Lorentzian matrix integral. After fixing the diagonal gauge for A_0, we parameterize the ordered eigenvalues holomorphically and define a time coordinate from the averaged eigenvalues of A_0. Using the band-diagonal structure of the spatial matrices in this basis, we construct block variables and evaluate time-dependent observables for the spatial geometry, including the spatial extent, its phase diagnostic, and the moment of inertia tensor. Since the fermionic Pfaffian can induce exceptionally large drifts when the fermion matrix develops near-zero modes, we introduce a fermionic mass parameter m_{f} as a regulator. In addition, to enhance fermionic effects while keeping the CLM under numerical control, we introduce an anisotropic deformation of the mass term. In the present work, the mass parameters γ and m_{f} are treated as auxiliary parameters, and the intended continuum approach is to take the large-N limit first and then explore the approach to $\gamma \to 0$ and $m_{\mathrm{f}} \to 0$.

For the bosonic model, in which the Pfaffian is replaced by a constant, we find that the time coordinate extracted from A_0 becomes approximately real at late times, while no spontaneous breaking of the spatial SO(9) symmetry is observed for the parameter set studied. Including fermions, we verify the band-diagonal structure of the spatial matrices, find that the spatial extent remains almost real, and observe a late-time expansion. For a representative parameter set, the eigenvalues of the moment of inertia tensor show that

three spatial directions become dominant at late times. In the present setup, where the deformation explicitly distinguishes the first $\tilde{d}$ directions from the remaining ones, this behavior suggests the emergence of a real, expanding $(3+1)$-dimensional spacetime.

The remainder of this thesis is organized as follows. Part I (Secs. 2–5) studies quantum decoherence in real-time path integrals, first in the Caldeira–Leggett model and then in a molecular toy model, with the complex-saddle results compared against the benchmark behavior. Part II (Secs. 6–10) reviews the Lorentzian IKKT matrix model, formulates the gauge-fixed Lorentzian setup and its CLM treatment, and presents numerical results for real-time observables extracted from matrix configurations. Sec. 10 summarizes the results and discusses future directions.

Part I

Quantum decoherence

2 Quantum decoherence

Quantum mechanics permits superpositions. Their physical signature is interference. For an isolated system, unitary time evolution preserves phase relations. In realistic situations, however, a system inevitably interacts with uncontrolled degrees of freedom—the environment—and this interaction generically creates entanglement. The central idea of decoherence is that, although the total "system + environment" state evolves unitarily, interference can be lost in the description based on the reduced density matrix, because the environment effectively stores information about relative phases.

To make this concrete, consider a system with position basis $\{|x\rangle\}$ and an environment initially prepared in a reference state $|\mathcal{E}_{\mathrm{ref}}\rangle$. Suppose that the interaction correlates different system configurations with different *environment records*. Starting from

$$|\Psi(0)\rangle = \left(\int dx\, \psi(x)\, |x\rangle\right) \otimes |\mathcal{E}_{\mathrm{ref}}\rangle\,, \tag{2.1}$$

the joint unitary evolution may be written schematically as

$$|\Psi(t)\rangle = \int dx\, \psi(x)\ |x\rangle \otimes |\mathcal{E}(x,t)\rangle\,, \tag{2.2}$$

where $|\mathcal{E}(x,t)\rangle$ denotes the environment record conditioned on the system being at position x.

The total density matrix is $\rho_{\rm SE}(t) = |\Psi(t)\rangle\langle\Psi(t)|$. An observer who accesses only the system describes it by the reduced density matrix

$$\rho_{\mathcal{S}}(t) = \mathrm{Tr}_{\rm E}\,\rho_{\rm SE}(t). \tag{2.3}$$

Using (2.2), its position-space matrix elements become

$$\begin{aligned}\rho_{\mathcal{S}}(x,\tilde{x};t) &\equiv \langle x|\,\rho_{\mathcal{S}}(t)\,|\tilde{x}\rangle \\ &= \psi(x)\,\psi^*(\tilde{x})\,\langle\mathcal{E}(\tilde{x},t)\mid\mathcal{E}(x,t)\rangle.\end{aligned} \tag{2.4}$$

If the environment records corresponding to different positions remain almost identical, $\langle\mathcal{E}(\tilde{x},t)\mid\mathcal{E}(x,t)\rangle \simeq 1$, the reduced density matrix retains coherence. In contrast, if the environment acquires (which-path) information so that records corresponding to different positions become nearly orthogonal,

$$\langle\mathcal{E}(\tilde{x},t)\mid\mathcal{E}(x,t)\rangle \approx 0 \qquad (x\neq\tilde{x}), \tag{2.5}$$

the off-diagonal elements of $\rho_{\mathcal{S}}(x,\tilde{x};t)$ are strongly suppressed.

In this way, decoherence appears as an effectively non-unitary evolution in the reduced description, even though the global time evolution remains unitary.

The same mechanism is transparent in a minimal two-level example. Assume that the system alternatives $|0\rangle$ and $|1\rangle$ become correlated with distinct environment records $|\mathcal{E}^{(0)}\rangle$ and $|\mathcal{E}^{(1)}\rangle$, respectively, so that

$$|\Psi\rangle_{SE} = \frac{1}{\sqrt{2}}\big(|0\rangle\,|\mathcal{E}^{(0)}\rangle + |1\rangle\,|\mathcal{E}^{(1)}\rangle\big), \qquad \rho_{SE} = |\Psi\rangle_{SE}\,\langle\Psi|_{SE}\,. \tag{2.6}$$

Tracing out the environment yields

$$\rho_{\mathcal{S}} = \mathrm{Tr}_{\rm E}\,\rho_{SE} = \frac{1}{2}\Big(|0\rangle\langle 0| + |1\rangle\langle 1| + \langle\mathcal{E}^{(1)}\mid\mathcal{E}^{(0)}\rangle\,|0\rangle\langle 1| + \langle\mathcal{E}^{(0)}\mid\mathcal{E}^{(1)}\rangle\,|1\rangle\langle 0|\Big). \tag{2.7}$$

In the $\{|0\rangle\,,|1\rangle\}$ basis, this reduced density matrix takes the form

$$\rho_{\mathcal{S}} = \frac{1}{2}\begin{pmatrix} 1 & \langle\mathcal{E}^{(1)}\mid\mathcal{E}^{(0)}\rangle \\ \langle\mathcal{E}^{(0)}\mid\mathcal{E}^{(1)}\rangle & 1 \end{pmatrix}. \tag{2.8}$$

The off-diagonal elements encode the coherence between the two system alternatives and are directly proportional to the overlap of the corresponding environment records. When $\langle\mathcal{E}^{(1)}\mid\mathcal{E}^{(0)}\rangle \to 0$, the reduced density matrix becomes approximately diagonal, and interference disappears in measurements performed on the system alone.

In this thesis we diagnose decoherence in the position basis. Namely, the suppression of off-diagonal matrix elements $\rho_{\mathcal{S}}(x,\tilde{x};t)$ with $x\neq\tilde{x}$ provides a direct and quantitative measure of decoherence. In the following sections, we analyze this suppression in concrete dynamical models and use it as the primary indicator of decoherence.

3 Brief review of the Caldeira–Leggett model

The Caldeira–Leggett (CL) model [1,2] provides a standard framework for describing dissipation and decoherence caused by coupling a system to an environment. While it was originally introduced for quantum Brownian motion, the same setup also leads to environment-induced decoherence [3]. In this section we briefly summarize the CL model and the path-integral formulation adopted in Ref. [4], which will be the starting point for our subsequent analysis of a molecular toy model. Throughout this section we set $\hbar = 1$.

3.1 Definition of the model

The CL model consists of a system $\mathcal{S}$ coupled linearly to an environment $\mathcal{E}$ made of $N_{\mathcal{E}}$ harmonic oscillators. The total Hamiltonian is

$$H = H_{\mathcal{S}} + H_{\mathcal{E}} + H_{\rm int}, \tag{3.1}$$

$$H_{\mathcal{S}} = \frac{p^2}{2M} + \frac{1}{2}M\omega_b^2 x^2, \tag{3.2}$$

$$H_{\mathcal{E}} = \sum_{k=1}^{N_{\mathcal{E}}} \left(\frac{(p^k)^2}{2m} + \frac{1}{2}m\omega_k^2 (q^k)^2 \right), \tag{3.3}$$

$$H_{\rm int} = -\, x \sum_{k=1}^{N_{\mathcal{E}}} c_k\, q^k. \tag{3.4}$$

Here ω_b denotes the bare frequency of the system oscillator; the corresponding renormalized frequency will appear after integrating out the environment.

We assume a factorized initial state,

$$\hat{\rho}(0) = \hat{\rho}_{\mathcal{S}}(0) \otimes \hat{\rho}_{\mathcal{E}}(0), \tag{3.5}$$

where the environment is initially in thermal equilibrium,

$$\hat{\rho}_{\mathcal{E}}(0) = \frac{e^{-\beta \hat{H}_{\mathcal{E}}}}{Z_{\mathcal{E}}}, \qquad Z_{\mathcal{E}} = \mathrm{Tr}_{\mathcal{E}}\; e^{-\beta \hat{H}_{\mathcal{E}}}. \tag{3.6}$$

Since the interaction is linear in x, it is convenient to work in the position basis. In particular, the bath density matrix at the initial time is written as

$$\rho_{\mathcal{E}}(q, \tilde{q}; 0) = \langle q | \hat{\rho}_{\mathcal{E}}(0) | \tilde{q} \rangle = \prod_{k=1}^{N_{\mathcal{E}}} \rho_{\mathcal{E}}^{(k)}(q^k, \tilde{q}^k; 0), \tag{3.7}$$

which will enter the influence-functional representation in the next subsection.

The density matrix of the full closed system evolves unitarily as

$$\rho(x,q;\tilde{x},\tilde{q};t) = \langle x,q|e^{-i\hat{H}t}\,\hat{\rho}(0)\,e^{i\hat{H}t}|\tilde{x},\tilde{q}\rangle\,. \tag{3.8}$$

The reduced density matrix of the system is then obtained by tracing out the environment at time t:

$$\rho_{\mathcal{S}}(x,\tilde{x};t) = \int dq\;\rho(x,q;\tilde{x},q;t) = \int dq\;\langle x,q|\hat{\rho}(t)|\tilde{x},q\rangle\,. \tag{3.9}$$

In the description based on the reduced density matrix, decoherence manifests itself as the suppression of off-diagonal elements in the position basis. In the following we focus on the realization used in Ref. [4] and set the microscopic couplings to be uniform, $c_k = c_{\mathrm{CL}}$ for $k = 1,\ldots,N_{\mathcal{E}}$.

3.2 Master equation in the Ohmic high-temperature limit

We now summarize the standard continuum description of decoherence in the Caldeira–Leggett model, keeping only the ingredients needed later for comparison with the finite-bath closed-system formulation adopted in this thesis. Starting from the reduced density matrix in the position basis, one may write its time evolution in terms of a reduced propagator as

$$\rho_{\mathcal{S}}(x_F,\tilde{x}_F;t) = \int dx_I\,d\tilde{x}_I\;J(x_F,\tilde{x}_F;t;x_I,\tilde{x}_I;0)\,\rho_{\mathcal{S}}(x_I,\tilde{x}_I;0). \tag{3.10}$$

In the path-integral formulation, the reduced propagator takes the form

$$J(x_F,\tilde{x}_F;t;x_I,\tilde{x}_I;0) = \int \mathcal{D}x\,\mathcal{D}\tilde{x}\;\exp\!\big\{i\big(S_{\mathcal{S}}[x]-S_{\mathcal{S}}[\tilde{x}]\big)\big\}\,e^{-W[x,\tilde{x}]}, \tag{3.11}$$

with the boundary conditions $x(0)=x_I$, $x(t)=x_F$, $\tilde{x}(0)=\tilde{x}_I$, and $\tilde{x}(t)=\tilde{x}_F$. Here

$$S_{\mathcal{S}}[x] = \int_0^t d\tau\,\left[\frac{1}{2}M\dot{x}(\tau)^2 - \frac{1}{2}M\omega_b^2 x(\tau)^2\right] \tag{3.12}$$

is the action of the bare system oscillator, while $e^{-W[x,\tilde{x}]}$ is the Feynman–Vernon influence functional [5] obtained after integrating out the environment.

For the thermal initial state introduced in the previous subsection, the influence phase can be written as

$$W[x,\tilde{x}] = \int_0^t d\tau\int_0^\tau ds\;\big(x(\tau)-\tilde{x}(\tau)\big)\Big(\alpha(\tau-s)\,x(s) - \alpha^*(\tau-s)\,\tilde{x}(s)\Big), \tag{3.13}$$

where the kernel $\alpha(\tau)$ is given by

$$\mathrm{Re}\,\alpha(\tau) = \int_0^\infty d\omega\;\frac{\rho(\omega)\,C(\omega)^2}{2m\omega}\coth\!\left(\frac{\beta\omega}{2}\right)\cos(\omega\tau), \tag{3.14}$$

$$\mathrm{Im}\,\alpha(\tau) = -\int_0^\infty d\omega\;\frac{\rho(\omega)\,C(\omega)^2}{2m\omega}\sin(\omega\tau). \tag{3.15}$$

It is convenient to separate

$$W[x,\tilde{x}] = W_R[x,\tilde{x}] + i\, W_I[x,\tilde{x}], \tag{3.16}$$

with

$$W_R[x,\tilde{x}] = \int_0^t d\tau \int_0^\tau ds\, \big(x(\tau)-\tilde{x}(\tau)\big)\, \mathrm{Re}\,\alpha(\tau-s)\, \big(x(s)-\tilde{x}(s)\big), \tag{3.17}$$

$$W_I[x,\tilde{x}] = \int_0^t d\tau \int_0^\tau ds\, \big(x(\tau)-\tilde{x}(\tau)\big)\, \mathrm{Im}\,\alpha(\tau-s)\, \big(x(s)+\tilde{x}(s)\big). \tag{3.18}$$

These expressions are nonlocal in time and encode the memory effect of the bath.

In the large-$N_{\mathcal{E}}$ limit, the environment is characterized by the spectral density. In the uniform-coupling realization used below ($c_k = c_{\mathrm{CL}}$), we introduce

$$\rho(\omega)\, C(\omega)^2 \equiv \sum_{k=1}^{N_{\mathcal{E}}} c_{\mathrm{CL}}^2\, \delta(\omega-\omega_k), \qquad C(\omega) = c_{\mathrm{CL}}. \tag{3.19}$$

The Ohmic setup with a high-frequency cutoff ω_{cut} is then specified by

$$\rho(\omega)\, C(\omega)^2 = \begin{cases} \dfrac{8mM\,\gamma_{CL}}{2\pi}\,\omega^2, & \omega \le \omega_{\mathrm{cut}}, \\ 0, & \omega > \omega_{\mathrm{cut}}, \end{cases} \tag{3.20}$$

which defines the effective damping parameter γ_{CL}.

To implement the Markov approximation, let us introduce

$$f(\tau) = \int_{-\omega_{\mathrm{cut}}}^{\omega_{\mathrm{cut}}} \frac{d\omega}{2\pi}\, \cos(\omega\tau). \tag{3.21}$$

When the relevant system dynamics is slow compared with the cutoff scale, one may approximate $f(\tau) \simeq \delta(\tau)$. Furthermore, in the high-temperature regime $\beta\omega_{\mathrm{cut}} \ll 1$, we may use $\coth(\beta\omega/2) \simeq 2/(\beta\omega)$. Under these assumptions, the nonlocal influence phase becomes effectively local:

$$W_I[x,\tilde{x}] \simeq -\frac{2M\gamma_{CL}\omega_{\mathrm{cut}}}{\pi} \int_0^t d\tau \left(x(\tau)^2 - \tilde{x}(\tau)^2\right) + M\gamma_{CL} \int_0^t d\tau \left(x(\tau)-\tilde{x}(\tau)\right)\left(\dot{x}(\tau)+\dot{\tilde{x}}(\tau)\right),$$

$$W_R[x,\tilde{x}] \simeq \frac{2M\gamma_{CL}}{\beta} \int_0^t d\tau \left(x(\tau)-\tilde{x}(\tau)\right)^2. \tag{3.22}$$

The first term in W_I can be absorbed into the system action by shifting the bare frequency. One thus obtains the renormalized frequency

$$\omega_r^2 = \omega_b^2 - \frac{4\gamma_{CL}\,\omega_{\mathrm{cut}}}{\pi}. \tag{3.23}$$

Denoting by $S_r[x]$ the action obtained from (3.12) by replacing ω_b with ω_r, the reduced propagator becomes

$$J(x_F,\tilde{x}_F;t;x_I,\tilde{x}_I;0)=\int \mathcal{D}x\,\mathcal{D}\tilde{x}\;\exp\!\Big\{iS_r[x]-iS_r[\tilde{x}]-iM\gamma_{CL}\int_0^t d\tau\,\big(x-\tilde{x}\big)\big(\dot{x}+\dot{\tilde{x}}\big)\Big\}$$
$$\times\exp\!\Big\{-\frac{2M\gamma_{CL}}{\beta}\int_0^t d\tau\,\big(x-\tilde{x}\big)^2\Big\}. \tag{3.24}$$

From this local form one obtains the Caldeira–Leggett master equation for the reduced density matrix in the position basis:

$$\frac{\partial}{\partial t}\rho_{\mathcal{S}}(x,\tilde{x};t)=K(x,\tilde{x})\,\rho_{\mathcal{S}}(x,\tilde{x};t), \tag{3.25}$$

where

$$K(x,\tilde{x})=\frac{i}{2M}\left(\partial_x^2-\partial_{\tilde{x}}^2\right)-\frac{i}{2}M\omega_r^2(x^2-\tilde{x}^2)$$
$$-\gamma_{CL}(x-\tilde{x})\left(\partial_x-\partial_{\tilde{x}}\right)-\frac{2M\gamma_{CL}}{\beta}(x-\tilde{x})^2. \tag{3.26}$$

The first two terms describe the unitary evolution with the renormalized oscillator frequency, the third term represents dissipation, and the last term drives the suppression of off-diagonal elements.

At sufficiently high temperature, the last term dominates the early-time behavior, and one finds

$$\rho_{\mathcal{S}}(x,\tilde{x};t)\sim\rho_{\mathcal{S}}(x,\tilde{x};0)\,\exp\!\left[-\frac{2M\gamma_{CL}}{\beta}(x-\tilde{x})^2t\right]. \tag{3.27}$$

This motivates the decoherence time

$$\tau_d^{-1}(x,\tilde{x})=\frac{2M\gamma_{CL}}{\beta}(x-\tilde{x})^2=\gamma_{CL}\left(\frac{x-\tilde{x}}{\lambda_{dB}}\right)^2,\qquad \lambda_{dB}=\sqrt{\frac{\beta}{2M}}, \tag{3.28}$$

where λ_{dB} is the thermal de Broglie wavelength. Thus, for fixed temperature and coupling, the off-diagonal components decay faster when the separation $|x-\tilde{x}|$ is larger.

The discussion above provides the continuum benchmark used throughout this part. In the next subsection, we explain how this benchmark is realized in the finite-bath discretization adopted for the full closed-system path integral.

3.3 Discrete bath parametrization and matching to the continuum benchmark

In order to connect the continuum benchmark reviewed above to the finite-bath model analyzed later in this thesis, we now specify how the environment with $N_{\mathcal{E}}$ oscillators is

discretized. The basic idea is to keep a finite number of environmental degrees of freedom, while choosing their frequency distribution and coupling strength so that the large-$N_{\mathcal{E}}$ limit reproduces the Ohmic continuum description.

We continue to use the uniform-coupling realization

$$c_k = c_{\rm CL} \qquad (k = 1, \ldots, N_{\mathcal{E}}), \tag{3.29}$$

introduced in the previous subsections. Since the continuum influence functional depends on the environment through the combination $\rho(\omega)C(\omega)^2$, fixing $C(\omega) = c_{\rm CL}$ leaves the nontrivial information in the distribution of the bath frequencies ω_k.

To reproduce the Ohmic form (3.20) in the large-$N_{\mathcal{E}}$ limit, we choose the bath frequencies as

$$\omega_k = \omega_{\rm cut} \left(\frac{k}{N_{\mathcal{E}}} \right)^{1/3} \qquad (k = 1, \ldots, N_{\mathcal{E}}). \tag{3.30}$$

Indeed, regarding $k/N_{\mathcal{E}}$ as a continuum variable, this choice implies

$$\rho(\omega) = \frac{dk}{d\omega} = \frac{3N_{\mathcal{E}}}{\omega_{\rm cut}^3}\, \omega^2 \qquad (\omega \le \omega_{\rm cut}), \tag{3.31}$$

and hence

$$\rho(\omega)\, C(\omega)^2 = \frac{3N_{\mathcal{E}}\, c_{\rm CL}^2}{\omega_{\rm cut}^3}\, \omega^2 \qquad (\omega \le \omega_{\rm cut}). \tag{3.32}$$

Comparing this with the continuum Ohmic form (3.20), one finds the large-$N_{\mathcal{E}}$ scaling

$$c_{\rm CL}^2 \sim \frac{4mM\,\gamma_{CL}}{3\pi N_{\mathcal{E}}}\, \omega_{\rm cut}^3. \tag{3.33}$$

For finite $N_{\mathcal{E}}$, however, it is more convenient to determine the microscopic coupling by matching the frequency renormalization directly. Starting from the Lagrangian corresponding to (3.1)–(3.4),

$$L = \frac{1}{2}M\dot{x}^2 - \frac{1}{2}M\omega_b^2 x^2 + \sum_{k=1}^{N_{\mathcal{E}}} \left(\frac{1}{2}m(\dot{q}^k)^2 - \frac{1}{2}m\omega_k^2 (q^k)^2 + c_{\rm CL}\, x\, q^k \right), \tag{3.34}$$

we complete the square with respect to q^k and obtain

$$L = \frac{1}{2}M\dot{x}^2 - \frac{1}{2}M\tilde{\omega}_r^2 x^2 + \sum_{k=1}^{N_{\mathcal{E}}} \left[\frac{1}{2}m(\dot{q}^k)^2 - \frac{1}{2}m\omega_k^2 \left(q^k - \frac{c_{\rm CL}}{m\omega_k^2} x \right)^2 \right], \tag{3.35}$$

where

$$\tilde{\omega}_r^2 = \omega_b^2 - \frac{c_{\rm CL}^2}{Mm} \sum_{k=1}^{N_{\mathcal{E}}} \frac{1}{\omega_k^2}. \tag{3.36}$$

Thus the finite bath induces a shift of the system frequency already at the microscopic level.

We now match this finite-$N_{\mathcal{E}}$ renormalized frequency to the continuum result obtained in the Ohmic high-temperature limit,

$$\omega_r^2 = \omega_b^2 - \frac{4\gamma_{CL}\,\omega_{\rm cut}}{\pi}. \tag{3.37}$$

Identifying $\tilde{\omega}_r = \omega_r$ and using (3.30), we arrive at

$$c_{\rm CL}^2 = \frac{4mM\,\gamma_{CL}}{\pi}\,\omega_{\rm cut}^3 \left\{ \sum_{k=1}^{N_{\mathcal{E}}} \left(\frac{N_{\mathcal{E}}}{k} \right)^{2/3} \right\}^{-1}. \tag{3.38}$$

This expression reduces to the asymptotic behavior (3.33) at large $N_{\mathcal{E}}$, since

$$\sum_{k=1}^{N_{\mathcal{E}}} \left(\frac{N_{\mathcal{E}}}{k} \right)^{2/3} \sim 3N_{\mathcal{E}} \qquad (N_{\mathcal{E}} \to \infty). \tag{3.39}$$

Therefore, for fixed $(\omega_{\rm cut}, N_{\mathcal{E}})$, the effective damping parameter scales as

$$\gamma_{CL} \propto c_{\rm CL}^2. \tag{3.40}$$

In the following subsection, we introduce the rescaled variables and the real-time discretization used to evaluate the path integral for the full closed system $\mathcal{S} + \mathcal{E}$.

3.4 Real-time path integral formulation (full closed system)

Having fixed the finite-bath parametrization in the previous subsection, we now formulate the unitary time evolution of the full closed system $\mathcal{S} + \mathcal{E}$ in the real-time path-integral language. Following Ref. [4], we work in the Lagrangian formulation and absorb the mass parameters by the rescaling

$$x \to \frac{x}{\sqrt{M}}, \qquad q^k \to \frac{q^k}{\sqrt{m}}, \qquad c_{\rm CL} \to c_{\rm CL}\sqrt{Mm}, \tag{3.41}$$

after which we drop the tildes on the rescaled variables. In what follows, the upper suffix k labels the k-th oscillator in the environment, while the lower suffix will be reserved for the discretized real-time index.

The Lagrangian is decomposed as

$$L = L_{\mathcal{S}} + L_{\mathcal{E}} + L_{\rm int}, \tag{3.42}$$

with

$$L_{\mathcal{S}} = \frac{1}{2}\dot{x}^{\,2} - \frac{1}{2}\omega_b^2 x^2, \tag{3.43}$$

$$L_{\mathcal{E}} = \sum_{k=1}^{N_{\mathcal{E}}} \left(\frac{1}{2}(\dot{q}^k)^2 - \frac{1}{2}\omega_k^2 (q^k)^2 \right), \tag{3.44}$$

$$L_{\rm int} = x \sum_{k=1}^{N_{\mathcal{E}}} c_{\rm CL}\, q^k. \tag{3.45}$$

The corresponding real-time action is

$$S[x,q] = \int_0^t d\tau \, \Big(L_{\mathcal{S}}[x(\tau)] + L_{\mathcal{E}}[q(\tau)] + L_{\rm int}[x(\tau), q(\tau)] \Big). \tag{3.46}$$

Thus the exact propagator for the full closed system can be written as

$$\langle x_F, q_F | e^{-i\hat{H}t} | x_I, q_I \rangle = \int \mathcal{D}x\, \mathcal{D}q \;\, \exp[iS[x,q]]\,, \tag{3.47}$$

with the boundary conditions $x(0) = x_I$, $x(t) = x_F$, $q(0) = q_I$, and $q(t) = q_F$. At this stage, the expression is simply an exact representation of the unitary time evolution of the closed system.

To evaluate this path integral numerically, we discretize the real time as

$$\tau_n = n\epsilon \qquad (n = 0, 1, \ldots, N_t), \qquad t = N_t \epsilon, \tag{3.48}$$

and define

$$x_n = x(\tau_n), \qquad q_n^k = q^k(\tau_n). \tag{3.49}$$

With this discretization, the action becomes a finite-dimensional quadratic form,

$$S(x,q) = S_{\mathcal{S}}(x) + S_{\mathcal{E}}(q) + S_{\rm int}(x,q), \tag{3.50}$$

where

$$S_{\mathcal{S}}(x) = \frac{\epsilon}{2} \sum_{n=0}^{N_t-1} \left[\left(\frac{x_{n+1} - x_n}{\epsilon} \right)^2 - \omega_b^2 \, \frac{x_n^2 + x_{n+1}^2}{2} \right], \tag{3.51}$$

$$S_{\mathcal{E}}(q) = \frac{\epsilon}{2} \sum_{k=1}^{N_{\mathcal{E}}} \sum_{n=0}^{N_t-1} \left[\left(\frac{q_{n+1}^k - q_n^k}{\epsilon} \right)^2 - \omega_k^2 \, \frac{(q_n^k)^2 + (q_{n+1}^k)^2}{2} \right], \tag{3.52}$$

$$S_{\rm int}(x,q) = \frac{c_{\rm CL}\,\epsilon}{2} \sum_{k=1}^{N_{\mathcal{E}}} \sum_{n=0}^{N_t-1} \left(x_n q_n^k + x_{n+1} q_{n+1}^k \right). \tag{3.53}$$

Here we have adopted a symmetric discretization for the potential and interaction terms, which is convenient for keeping the action quadratic in the discretized variables and for taking the continuum limit $\epsilon \to 0$.

Accordingly, the real-time propagator is represented by an ordinary multiple integral over the intermediate variables,

$$\langle x_F, q_F | e^{-i\hat{H}t} | x_I, q_I \rangle = \int \left(\prod_{n=1}^{N_t-1} dx_n \right) \left(\prod_{k=1}^{N_\mathcal{E}} \prod_{n=1}^{N_t-1} dq_n^k \right) \exp[iS(x,q)] \,, \tag{3.54}$$

where the endpoints are fixed as

$$x_0 = x_I, \qquad x_{N_t} = x_F, \qquad q_0^k = q_I^k, \qquad q_{N_t}^k = q_F^k. \tag{3.55}$$

The next step is to duplicate the real-time paths into forward and backward branches and to combine them with the initial density matrices of the system and the environment. This yields a closed-system path-integral representation of the reduced density matrix, which will be the starting point for the Gaussian saddle-point analysis in the subsequent subsections.

3.5 Reduced density matrix as a closed-system path integral

Using the discretized real-time propagator introduced in the previous subsection, we now construct a path-integral representation of the reduced density matrix for the system $\mathcal{S}$. By tracing out the environment at the final time, the reduced density matrix (3.9) is written in the discretized closed-system formulation as

$$\rho_\mathcal{S}(x_F, \tilde{x}_F; t) = \int \mathcal{D}x \, \mathcal{D}\tilde{x} \prod_{k=1}^{N_\mathcal{E}} \mathcal{D}q^k \, \mathcal{D}\tilde{q}^k \; \rho_\mathcal{S}(x_0, \tilde{x}_0; 0) \prod_{k=1}^{N_\mathcal{E}} \rho_\mathcal{E}^{(k)}(q_0^k, \tilde{q}_0^k; 0) \; \exp[i\{S(x,q) - S(\tilde{x},\tilde{q})\}] \,. \tag{3.56}$$

Here the forward and backward system paths satisfy

$$x_{N_t} = x_F, \qquad \tilde{x}_{N_t} = \tilde{x}_F, \tag{3.57}$$

while the trace over the environment is implemented by identifying the final configurations on the two branches,

$$q_{N_t}^k = \tilde{q}_{N_t}^k \qquad (k = 1, \ldots, N_\mathcal{E}), \tag{3.58}$$

and integrating over these common final values.

As an initial condition for the system $\mathcal{S}$, we take a Gaussian wave packet,

$$\rho_{\mathcal{S}}(x,\tilde{x};0) = \psi_I(x)\,\psi_I^*(\tilde{x}), \tag{3.59}$$

$$\psi_I(x) = \exp\!\left(-\frac{x^2}{4\sigma^2}\right). \tag{3.60}$$

The environment $\mathcal{E}$ is initially in the canonical ensemble at inverse temperature β. For later numerical treatment, it is convenient to represent the thermal density matrix by an additional path in the imaginary-time direction. Discretizing the Euclidean time as

$$\beta = N_\beta \tilde{\epsilon}, \tag{3.61}$$

we define

$$\tilde{q}_0^k(j) \equiv \tilde{q}^k(-i\,j\tilde{\epsilon}) \qquad (j = 0, 1, \ldots, N_\beta). \tag{3.62}$$

The corresponding free Euclidean action of the bath is

$$S_0(\tilde{q}_0) = \frac{1}{2}\,\tilde{\epsilon} \sum_{k=1}^{N_{\mathcal{E}}} \sum_{j=0}^{N_\beta - 1} \left[\left(\frac{\tilde{q}_0^k(j+1) - \tilde{q}_0^k(j)}{\tilde{\epsilon}} \right)^2 + \omega_k^2\, \frac{\tilde{q}_0^k(j+1)^2 + \tilde{q}_0^k(j)^2}{2} \right], \tag{3.63}$$

with the boundary conditions

$$\tilde{q}_0^k(0) = \tilde{q}_0^k, \qquad \tilde{q}_0^k(N_\beta) = q_0^k. \tag{3.64}$$

Combining the forward/backward real-time paths with the imaginary-time path for the thermal initial state, we can rewrite the reduced density matrix as

$$\rho_{\mathcal{S}}(x_F,\tilde{x}_F;t) = \int \mathcal{D}x\,\mathcal{D}\tilde{x} \prod_{k=1}^{N_{\mathcal{E}}} \mathcal{D}q^k\,\mathcal{D}\tilde{q}^k\,\mathcal{D}\tilde{q}_0^k\ \exp[-S_{\text{eff}}(x,\tilde{x},q,\tilde{q},\tilde{q}_0)]\,, \tag{3.65}$$

where the effective action is

$$S_{\text{eff}}(x,\tilde{x},q,\tilde{q},\tilde{q}_0) = -i\Big\{ S(x,q) - S(\tilde{x},\tilde{q}) \Big\} + S_0(\tilde{q}_0) + \frac{1}{4\sigma^2}\left(x_0^2 + \tilde{x}_0^2\right). \tag{3.66}$$

The first term is purely imaginary, whereas the last two terms are real. Therefore the integrand of (3.65) is complex, and a naive Monte Carlo evaluation suffers from the sign problem. On the other hand, for the CL model with the Gaussian initial state chosen above, S_{eff} is quadratic in all integration variables. The path integral (3.65) therefore reduces to a finite-dimensional Gaussian integral, which will be evaluated explicitly in the next subsection.

3.6 Gaussian structure and saddle-point evaluation

As emphasized in the previous subsection, the effective action (3.66) is quadratic in all integration variables. Therefore the reduced density matrix (3.65) can be evaluated exactly as a finite-dimensional Gaussian integral.

To make this structure explicit, we collect all independent integration variables into a single vector

$$X_I, \qquad I = 1, \ldots, N_{\rm var}. \tag{3.67}$$

A convenient choice is given by

- the system variables $x_n, \tilde{x}_n$ for $n = 0, 1, \ldots, N_t - 1$, with $x_{N_t} = x_F$ and $\tilde{x}_{N_t} = \tilde{x}_F$ fixed,
- the real-time environment variables $q_n^k, \tilde{q}_n^k$ subject to the final-time identification $q_{N_t}^k = \tilde{q}_{N_t}^k$,
- the imaginary-time bath variables $\tilde{q}_0^k(j)$ for $j = 1, 2, \ldots, N_\beta - 1$, with endpoints fixed by $\tilde{q}_0^k(0) = \tilde{q}_0^k$ and $\tilde{q}_0^k(N_\beta) = q_0^k$.

With this convention, the total number of independent integration variables is

$$N_{\rm var} = 2N_t(1 + N_{\mathcal{E}}) + N_\beta N_{\mathcal{E}}. \tag{3.68}$$

In terms of X_I, the effective action can be written as

$$S_{\rm eff} = \frac{1}{2} X_I M_{IJ} X_J - C_I X_I + B, \tag{3.69}$$

where M_{IJ} is an $N_{\rm var} \times N_{\rm var}$ complex symmetric matrix, C_I is linear in the final coordinates $(x_F, \tilde{x}_F)$, and B depends only on $(x_F, \tilde{x}_F)$. Because the discretized action is local in the time-slice index, the matrix M_{IJ} is sparse even though its size becomes large.

Since the endpoint dependence enters linearly, it is convenient to decompose

$$C_I = i\big(x_F\, c_I - \tilde{x}_F\, \tilde{c}_I\big), \tag{3.70}$$

which defines the coefficient vectors c_I and $\tilde{c}_I$. In the present discretization, B is purely imaginary, so the $(x_F, \tilde{x}_F)$ dependence relevant for the magnitude of the reduced density matrix comes entirely from the quadratic term generated by the Gaussian integration.

The saddle point is determined by the stationary condition

$$\frac{\partial S_{\rm eff}}{\partial X_I} = 0, \qquad \Longrightarrow \qquad M_{IJ}\, \bar{X}_J = C_I. \tag{3.71}$$

Thus the relevant saddle is obtained by solving the linear system

$$\bar{X}_I = (M^{-1})_{IJ} C_J. \tag{3.72}$$

In general this saddle lies at complex values of the integration variables, which is the origin of the complex-saddle interpretation of the reduced density matrix.

Shifting the integration variables as

$$X_I = \bar{X}_I + Y_I, \tag{3.73}$$

the effective action becomes

$$S_{\text{eff}} = \frac{1}{2} Y_I M_{IJ} Y_J + \left(B - \frac{1}{2} C_I (M^{-1})_{IJ} C_J \right). \tag{3.74}$$

Since the shifted action is purely quadratic in Y_I, the integration over the corresponding Lefschetz thimble reduces to the evaluation of a Gaussian integral. Therefore the path integral (3.65) reduces to

$$\rho_{\mathcal{S}}(x_F, \tilde{x}_F; t) = \frac{1}{\sqrt{\det M}} \exp[-A(x_F, \tilde{x}_F; t)], \tag{3.75}$$

with

$$A(x_F, \tilde{x}_F; t) = B - \frac{1}{2} C_I (M^{-1})_{IJ} C_J. \tag{3.76}$$

The prefactor $1/\sqrt{\det M}$ is independent of $(x_F, \tilde{x}_F)$ and therefore does not affect the discussion of decoherence itself.

Equation (3.75) shows that the reduced density matrix retains a Gaussian form at all times. For the purpose of diagnosing decoherence, the essential information is therefore contained in the quadratic dependence of $\mathrm{Re}\, A$ on the final coordinates. In the next subsection, we use the decomposition (3.70) to extract from $\mathrm{Re}\, A$ the coefficients that govern the fall-off of the reduced density matrix along the diagonal and off-diagonal directions in the position basis.

3.7 Decoherence diagnostics from the Gaussian reduced density matrix

Equation (3.75) shows that the reduced density matrix retains a Gaussian form. To probe decoherence, we therefore focus on the magnitude $|\rho_{\mathcal{S}}(x_F, \tilde{x}_F; t)|$, which is governed by $\mathrm{Re}\, A$.

Using the decomposition (3.70) introduced in the previous subsection, together with (3.76), we can parametrize

$$\mathrm{Re}\, A = \frac{1}{2}\begin{pmatrix} x_F & \tilde{x}_F \end{pmatrix}\begin{pmatrix} J & -K \\ -K & J \end{pmatrix}\begin{pmatrix} x_F \\ \tilde{x}_F \end{pmatrix} = \frac{1}{4}\Big\{(J-K)(x_F+\tilde{x}_F)^2 + (J+K)(x_F-\tilde{x}_F)^2\Big\}, \tag{3.77}$$

where

$$J \equiv \mathrm{Re}\big\{c_I (M^{-1})_{IJ} c_J\big\} = \mathrm{Re}\big\{\tilde{c}_I (M^{-1})_{IJ} \tilde{c}_J\big\}\,, \tag{3.78}$$

$$K \equiv \mathrm{Re}\big\{c_I (M^{-1})_{IJ} \tilde{c}_J\big\} = \mathrm{Re}\big\{\tilde{c}_I (M^{-1})_{IJ} c_J\big\}\,. \tag{3.79}$$

Here c_I and $\tilde{c}_I$ are the endpoint coefficient vectors defined in (3.70). The fact that the same coefficient J appears in the two diagonal entries follows from the Hermiticity of the reduced density matrix, $\rho_{\mathcal{S}}(x_F, \tilde{x}_F; t) = \rho^*_{\mathcal{S}}(\tilde{x}_F, x_F; t)$, which implies that $\mathrm{Re}\, A$ is invariant under the exchange $x_F \leftrightarrow \tilde{x}_F$.

The fall-off along the diagonal and off-diagonal directions is then characterized by

$$\Gamma_{\text{diag}}(t) \equiv 2(J-K), \tag{3.80}$$

$$\Gamma_{\text{off-diag}}(t) \equiv 2(J+K). \tag{3.81}$$

Thus, up to an $(x_F, \tilde{x}_F)$-independent prefactor,

$$|\rho_{\mathcal{S}}(x_F, \tilde{x}_F; t)| \simeq \exp\left[-\frac{1}{2}\Gamma_{\text{diag}}(t)\left(\frac{x_F+\tilde{x}_F}{2}\right)^2 - \frac{1}{2}\Gamma_{\text{off-diag}}(t)\left(\frac{x_F-\tilde{x}_F}{2}\right)^2\right]. \tag{3.82}$$

In particular, $\Gamma_{\text{off-diag}}(t)$ directly quantifies the suppression of off-diagonal elements in the position basis.

The continuum benchmark derived in Sec. 3.2 predicts that, at high temperature and at early times, the off-diagonal damping behaves as

$$|\rho_{\mathcal{S}}(x_F, \tilde{x}_F; t)| \sim \exp\left[-\frac{2\gamma_{CL}}{\beta}(x_F-\tilde{x}_F)^2\, t\right] \tag{3.83}$$

in the rescaled convention (3.41). Comparing this expression with (3.82), we obtain the early-time expectation

$$\Gamma_{\text{off-diag}}(t) \sim \frac{16\gamma_{CL}}{\beta}\, t, \qquad (t \text{ small}). \tag{3.84}$$

This is the quantity that can be extracted directly from the exact closed-system path integral and compared with the standard master-equation prediction.

Furthermore, the finite-bath matching discussed in Sec. 3.3 implies that, for fixed $(\omega_{\rm cut}, N_{\mathcal{E}})$, one has

$$\gamma_{CL} \propto c_{CL}^2. \tag{3.85}$$

Therefore the same benchmark may be written as

$$\Gamma_{\text{off-diag}}(t) \propto \frac{c_{CL}^2}{\beta}\, t \qquad \text{for fixed } (\omega_{\rm cut}, N_{\mathcal{E}}). \tag{3.86}$$

This scaling relation will be useful later when we discuss how the decoherence diagnostic depends on the coupling strength and the inverse temperature in our molecular toy model.

In Ref. [4], the early-time linear growth (3.84) was confirmed by evaluating the full closed-system real-time path integral without relying on the local master equation itself. The important point is that the same quantity can be extracted from the unitary time evolution of the full system $\mathcal{S}+\mathcal{E}$, and therefore its agreement with the continuum prediction does not rely on reusing the Markov or high-temperature approximations at the numerical stage. In later sections, we adopt the same diagnostics for our toy model that mimics a molecular system.

4 Decoherence in large molecules

In Sec. 3, we reviewed the Caldeira–Leggett (CL) model as a benchmark for environment-induced decoherence and introduced the reduced-density-matrix diagnostic $\Gamma_{\text{off-diag}}(t)$. We now turn to a different setting and consider a toy model intended to mimic a large molecular system. Our purpose here is not to reproduce the CL model exactly, but to construct a simple Gaussian model in which a distinguished collective degree of freedom is coupled to many other degrees of freedom, so that the same framework can be used to analyze decoherence.

A full microscopic treatment of decoherence in large molecules is in general difficult, since one must deal with many internal degrees of freedom as well as their coupling to external environments. For this reason, it is useful to introduce a simplified model that captures the coexistence of collective motion and internal dynamics while remaining analytically and numerically tractable. In the present section, we use a three-dimensional lattice model for this purpose.

The basic idea is to regard the center-of-mass (CM) coordinate as the distinguished degree of freedom and the internal relative coordinates as the sector coupled to it. This internal sector is not an external bath as in the CL model, but it can still play an analogous role when one studies the reduced density matrix of the CM coordinate. In particular, we

use the pinning strength c as the corresponding control parameter for the coupling strength, and later compare its effect on $\Gamma_{\text{off-diag}}(t)$ with the benchmark behavior reviewed in Sec. 3.

4.1 A toy model of a molecule

We consider a three-dimensional lattice model with nearest-neighbour interactions. The coordinates of the N particles are denoted by $x_\mu^{(p)}(t)$, where $p = 1, \ldots, N$ labels the particles and $\mu = 1, 2, 3$ is the spatial index. The total number of sites is taken to be $N = N_s^3$. The interaction potential is

$$V(x) = \frac{\lambda}{2} \sum_{\langle p,q \rangle} \sum_{\mu=1}^{3} \big(x_\mu^{(p)} - x_\mu^{(q)}\big)^2, \tag{4.1}$$

where the sum $\sum_{\langle p,q \rangle}$ runs over all nearest-neighbour pairs on the cubic lattice. The action is

$$S[x] = \int dt\; L[x], \qquad L[x] = \sum_{p=1}^{N} \sum_{\mu=1}^{3} \frac{m}{2} \big(\dot{x}_\mu^{(p)}\big)^2 - V(x). \tag{4.2}$$

It is convenient to introduce the center-of-mass (CM) and relative coordinates. We define the CM coordinate as

$$X_\mu = \frac{1}{N} \sum_{p=1}^{N} x_\mu^{(p)}, \tag{4.3}$$

and the relative coordinates by

$$\xi_\mu^{(p)} = x_\mu^{(p)} - X_\mu, \qquad \sum_{p=1}^{N} \xi_\mu^{(p)} = 0. \tag{4.4}$$

Since the interaction is written entirely in terms of coordinate differences, the CM and relative coordinates are decoupled in the original unpinned model.

To induce a coupling between the CM motion and the internal relative sector, we introduce a pinning potential at a distinguished site, which we choose to be $p = N$:

$$V_{\text{pin}}(x) = \frac{c}{2} \sum_{\mu=1}^{3} \big(x_\mu^{(N)}\big)^2. \tag{4.5}$$

Here the parameter c plays the role of the coupling-strength parameter in the toy model. In particular, after rewriting the theory in terms of the CM and relative coordinates, c controls how strongly the distinguished CM degree of freedom is coupled to the internal sector, and it is therefore the natural quantity to compare with the microscopic coupling c_{CL} in the CL benchmark.

In terms of X_μ and $\xi_\mu^{(p)}$, the Lagrangian becomes

$$L = \sum_{p=1}^{N}\sum_{\mu=1}^{3}\frac{m}{2}\big(\dot{\xi}_\mu^{(p)}\big)^2 + \sum_{\mu=1}^{3}\frac{mN}{2}\big(\dot{X}_\mu\big)^2 - \frac{c}{2}\sum_{\mu=1}^{3}\big(\xi_\mu^{(N)}\big)^2 - c\sum_{\mu=1}^{3}\xi_\mu^{(N)}X_\mu - \frac{c}{2}\sum_{\mu=1}^{3}\big(X_\mu\big)^2 - \frac{\lambda}{2}\sum_{\langle p,q\rangle}\sum_{\mu=1}^{3}\big(\xi_\mu^{(p)} - \xi_\mu^{(q)}\big)^2. \tag{4.6}$$

Thus the pinning term has two effects: it introduces a direct quadratic term for the CM coordinate, and at the same time it generates a linear coupling between the CM coordinate and the relative coordinate at the pinned site. This coupling is the origin of the decoherence channel that we investigate below.

By rescaling x and t, we set $m = 1$ and $\lambda = 1$ in what follows. In addition, we rescale $X_\mu \to \frac{1}{\sqrt{N}}X_\mu$ so that the kinetic term becomes $\frac{1}{2}\dot{X}_\mu^2$. Using the discrete Laplacian matrix H_{pq}, the Lagrangian can be written as

$$L = \sum_{p=1}^{N}\sum_{\mu=1}^{3}\frac{1}{2}\big(\dot{\xi}_\mu^{(p)}\big)^2 + \sum_{\mu=1}^{3}\frac{1}{2}\dot{X}_\mu^2 - \sum_{\mu=1}^{3}\frac{c}{2}\big(\xi_\mu^{(N)}\big)^2 - \sum_{\mu=1}^{3}\frac{c}{\sqrt{N}}\,\xi_\mu^{(N)}X_\mu - \sum_{\mu=1}^{3}\frac{c}{2N}X_\mu^2 - \frac{1}{2}\sum_{\mu=1}^{3}\sum_{p,q=1}^{N}\xi_\mu^{(p)}H_{pq}\,\xi_\mu^{(q)}, \tag{4.7}$$

where the last term describes the quadratic internal dynamics of the relative sector.

Correspondingly, the action can be decomposed as

$$S = S_{\mathcal{S}}[X] + S_{\mathcal{E}}[\xi] + S_{\mathrm{int}}[X,\xi]\,. \tag{4.8}$$

This decomposition makes the analogy with Sec. 3 transparent: the CM coordinate plays the role of the distinguished system variable, while the relative coordinates play the role of the sector coupled to it. The microscopic structure is different from that of the CL model, but this is sufficient for the present purpose of comparing how the decoherence diagnostic depends on the coupling-strength parameter.

4.2 Renormalized center-of-mass frequency

The pinning term in (4.7) induces a linear coupling between the CM coordinate X_μ and the relative coordinates $\xi_\mu^{(p)}$. Since the model is Gaussian, the relative sector can be integrated out exactly, after properly imposing the constraint $\sum_p \xi_\mu^{(p)} = 0$. This generates an effective quadratic term for the CM coordinate and hence a renormalized CM frequency.

Since the three spatial components decouple and are equivalent, we suppress the index μ in the following and consider one representative component. The renormalized CM

frequency can then be written as

$$\omega_r^2 = \frac{c}{N(1 + c\, s_0)}. \tag{4.9}$$

Here s_0 is a positive constant determined solely by the relative sector and the choice of the pinned site for a given lattice size and pinning setup, and it is independent of the pinning strength c. In practice, s_0 can be treated as a precomputable constant. All definitions and the derivation of (4.9) are given in Appendix B.

Completing the square for the internal normal modes, one finds that the CM coordinate acquires a renormalized quadratic term. Namely, keeping only the CM part, the effective Lagrangian becomes

$$L_{\mathrm{CM}} = \frac{1}{2}\dot{X}^2 - \frac{1}{2}\omega_r^2 X^2, \qquad \omega_r^2 = \omega_r^2(c). \tag{4.10}$$

In the CL setup reviewed in Sec. 3, the microscopic coupling c_{CL} controls the interaction between the distinguished system coordinate and the bath. In the present molecular toy model, we use the pinning strength c as the corresponding control parameter, since it determines how strongly the CM coordinate is coupled to the internal relative degrees of freedom. Our purpose is not to realize the CL setup exactly, but to use it as a benchmark and compare how the decoherence diagnostic depends on the coupling strength in the toy model. From this viewpoint, it is natural to compare c with c_{CL}.

Unlike the CL case, however, the same parameter c also changes the renormalized CM frequency $\omega_r = \omega_r(c)$ through (4.9). Thus, in the present toy model, the coupling-strength parameter and the effective CM frequency are not independent. This is a model-specific feature that should be kept in mind in later comparisons with the CL benchmark.

Nevertheless, once $\omega_r(c)$ is fixed, the subsequent analysis follows the same general strategy as in Sec. 3: we construct the reduced density matrix for the CM coordinate, use the Gaussian structure of the model, and extract the decoherence diagnostic from the resulting quadratic form. In this sense, what is carried over from the CL discussion is the reduced-density-matrix framework and the diagnostic $\Gamma_{\text{off-diag}}(t)$, while the microscopic origin of the coupled sector is specific to the present toy model.

Since the next section specifies the initial CM state, we choose it for each value of c so that it coincides with the ground-state wave packet of the harmonic oscillator with frequency $\omega_r(c)$.

5 Numerical results for a Gaussian wave packet

We now present numerical results for the molecular toy model introduced in Sec. 4. The full system evolves unitarily as a closed system, but the CM mode becomes effectively

mixed once the internal relative modes are traced out. Following the reduced-density-matrix framework reviewed in Sec. 3, we diagnose decoherence through the suppression of off-diagonal elements in the position basis and through the quantity $\Gamma_{\text{off-diag}}(t)$ extracted from the Gaussian form of the reduced density matrix.

5.1 Initial condition: Gaussian wave packet

We prepare the initial density matrix of the CM mode as a pure state

$$\rho_{\mathcal{S}}(X, \tilde{X}; 0) = \psi_I(X)\, \psi_I^*(\tilde{X}), \tag{5.1}$$

with the Gaussian wave packet

$$\psi_I(X) = \exp\left(-\frac{X^2}{4\sigma^2}\right). \tag{5.2}$$

We choose the width as $\sigma^2 = 1/(2\omega_r)$ so that $\psi_I(X)$ coincides with the ground-state wave packet of the harmonic oscillator with renormalized frequency $\omega_r = \omega_r(c)$ determined by the pinning coupling c through (4.9). The internal relative modes, which are traced out in constructing the reduced density matrix of the CM coordinate, are taken to be in thermal equilibrium at inverse temperature β.

5.2 Disappearance of off-diagonal components

Using the Gaussian initial state (5.2) for the CM mode and a thermal initial state for the internal relative modes, we first examine the time evolution of the reduced density matrix itself. In the representative parameter set used in Fig. 1, we choose $N = 64$, $c = 3.0$, and $\beta = 0.05$. With this setup, the off-diagonal region of the reduced density matrix is rapidly suppressed in the time interval $t \simeq 0$–1, while the diagonal ridge remains. We interpret this as a direct numerical manifestation of decoherence in the position basis.

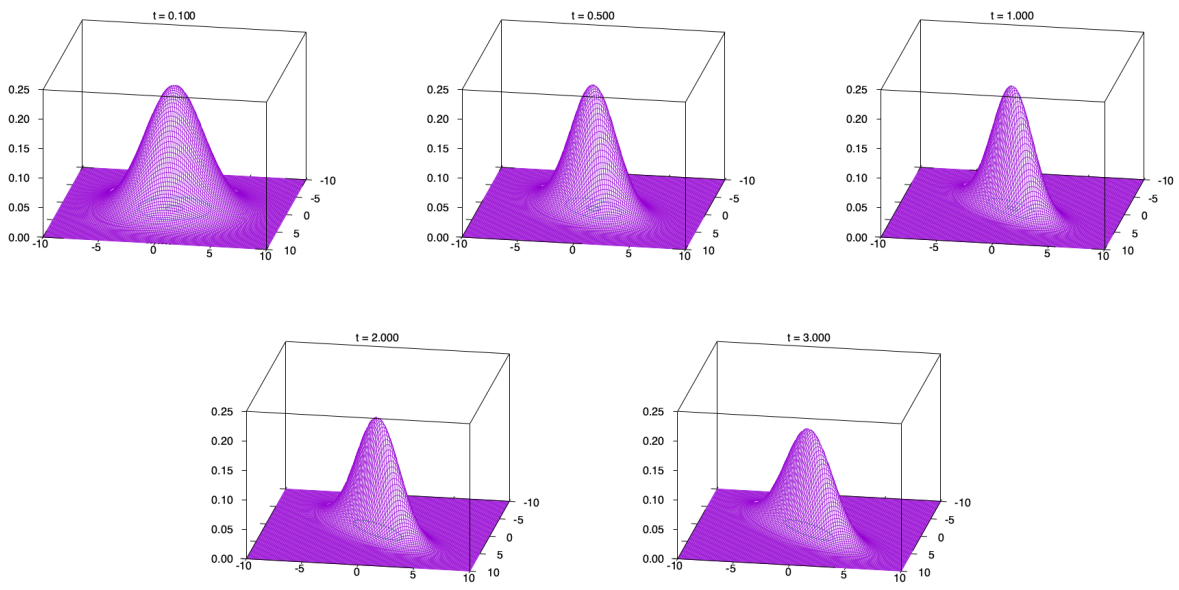

Figure 1: Suppression of off-diagonal components of the reduced density matrix in the lattice model for $N = 64$, $c = 3.0$, and $\beta = 0.05$.

5.3 Dependence on coupling and inverse temperature

To quantify the off-diagonal suppression more systematically, we extract $\Gamma_{\text{off-diag}}(t)$ from the Gaussian form of the reduced density matrix in the same way as in Sec. 3.7, namely as the coefficient governing the fall-off of $|\rho_S(X, \tilde{X}; t)|$ along the off-diagonal direction. We then study how this quantity depends on the pinning coupling c and the inverse temperature β, with the Gaussian width fixed by $\omega_r(c)$ through (4.9). Unless stated otherwise, we fix the lattice size to $N = 27$ and vary (i) the coupling c and (ii) the inverse temperature β.

The observed trend is that increasing c and decreasing β both make the off-diagonal components decay faster, indicating more efficient decoherence in these parameter directions.

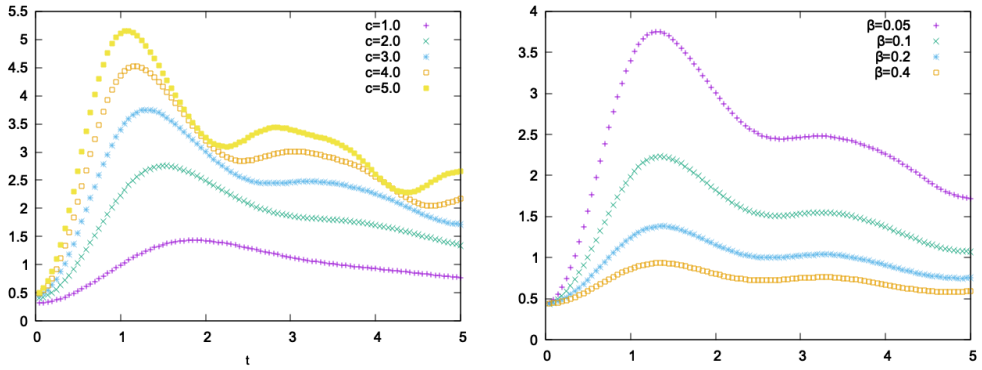

Figure 2: Parameter dependence of the off-diagonal suppression: (left) c dependence at fixed β, and (right) β dependence at fixed c.

To visualize the expected early-time scaling, we consider the rescaled quantity

$$\tilde{\Gamma}(t) \equiv \frac{\beta}{c}\left\{\Gamma_{\text{off-diag}}(t) - \Gamma_{\text{off-diag}}(0)\right\}, \tag{5.3}$$

which removes the offset at $t = 0$ and factors out the explicit c/β dependence suggested by the data. If $\Gamma_{\text{off-diag}}(t)$ behaves as

$$\Gamma_{\text{off-diag}}(t) \simeq A\,\frac{c}{\beta}\,t + B \qquad (t \text{ small}), \tag{5.4}$$

then $\tilde{\Gamma}(t)$ should show an approximately universal early-time slope, $\tilde{\Gamma}(t) \simeq A\,t$, independent of c and β in the parameter region where this scaling holds.

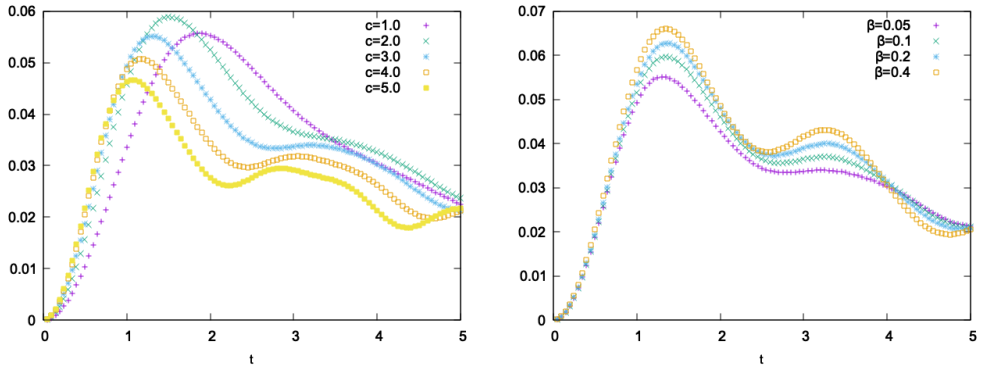

Figure 3: Plots of $\tilde{\Gamma}(t)$ defined in (5.3): (left) c dependence at fixed β, and (right) β dependence at fixed c.

To quantify the coefficient A, we fit the early-time behavior of $\Gamma_{\text{off-diag}}(t)$ by a linear function $f(t) = a\,t + b$ in an interval where the data are well described by a straight line.

We then plot the fitted slope a as a function of the combination c/β. If (5.4) holds, the slope should scale as $a \simeq A\,(c/\beta)$, and hence A can be extracted from a linear fit of a versus c/β in the appropriate large-c or small-β regime.

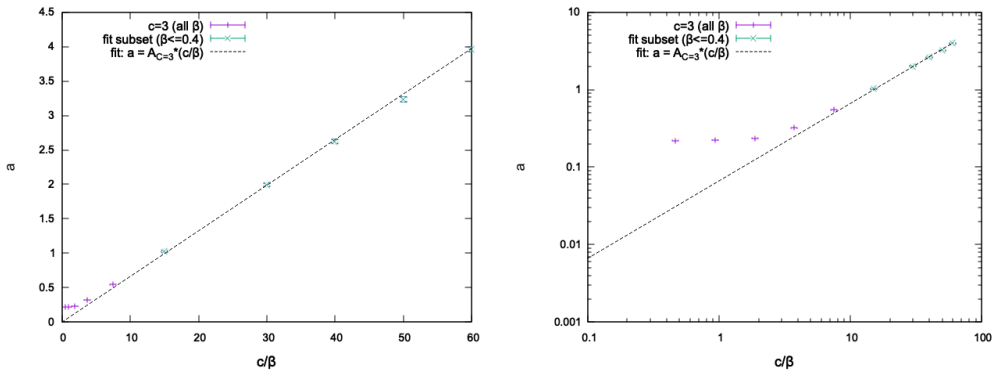

Figure 4: Fitted slope a of $\Gamma_{\text{off-diag}}(t)$ at early time as a function of c/β for several β at fixed $c = 3.0$. The log–log plot indicates the region where the small-β scaling sets in.

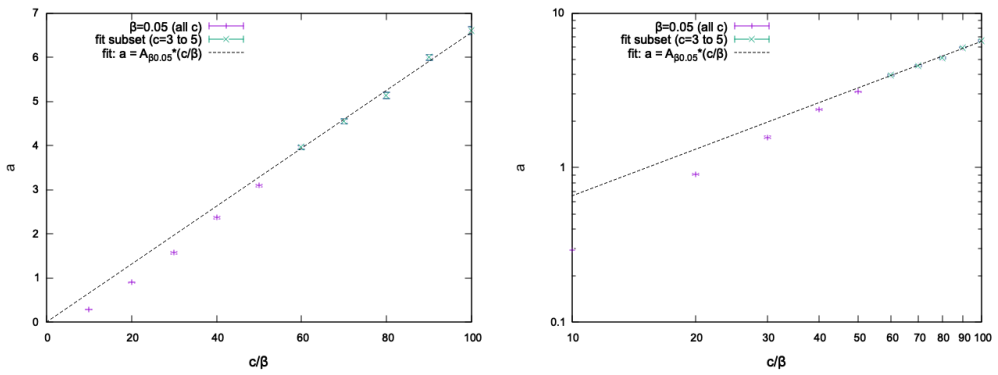

Figure 5: Fitted slope a of $\Gamma_{\text{off-diag}}(t)$ at early time as a function of c/β for several c at fixed $\beta = 0.05$ ($\beta^{-1} = 20$). The log–log plot indicates the region where the large-c scaling sets in.

From the linear fits of a versus c/β in the small-β (fixed $c = 3.0$) and large-c (fixed $\beta = 0.05$) regimes, we obtain

$$A_{c=3.0} = 0.06625 \pm 0.0005982, \qquad A_{\beta=0.05} = 0.06568 \pm 0.0004088. \tag{5.5}$$

These two determinations agree within the error bars, and we therefore quote a representative value

$$A \simeq 6.60 \times 10^{-2}\,. \tag{5.6}$$

This provides a quantitative confirmation of the early-time scaling form (5.4) in the region where the linear regime is observed.

Finally, we emphasize that the coupling dependence in our lattice model is not expected to coincide with that of the CL model. In the CL setup, the continuum benchmark is (3.84), namely $\Gamma_{\text{off-diag}}(t) \sim (16\gamma_{CL}/\beta)\, t$ at high temperature, where γ_{CL} is the effective damping parameter defined through the Ohmic spectral density. In the uniform-coupling realization reviewed in Sec. 3.3, one has $\gamma_{CL} \propto c_{\text{CL}}^2$ for fixed $(\omega_{\text{cut}}, N_{\mathcal{E}})$, so that the CL benchmark implies $\Gamma_{\text{off-diag}}(t) \propto (c_{\text{CL}}^2/\beta)\, t$ at early time.

In contrast, in our lattice model we observe the scaling $\Gamma_{\text{off-diag}}(t) \propto (c/\beta)\, t$ in the regime studied here. This difference from the CL benchmark suggests that decoherence in a composite system with many internal degrees of freedom can exhibit a qualitatively different dependence on the microscopic coupling parameter from that in a point-like system coupled to an external bath. From this point of view, the present result may be interpreted as a characteristic feature of the molecular setting modeled here, and it motivates further investigation of decoherence specific to large molecules.

Part II

The beginning of the universe

6 Brief review of the IKKT matrix model

In this section we review the IKKT matrix model, which was proposed as a candidate for a nonperturbative formulation of superstring theory [6]. This model is obtained by dimensionally reducing ten-dimensional $\mathcal{N} = 1$ super Yang–Mills theory to zero dimensions. One of the most attractive aspects of the IKKT matrix model is that spacetime does not exist a priori, but is expected to emerge from the matrix degrees of freedom. This feature motivates studying the beginning of the universe within a framework of superstring theory beyond perturbation theory. In this section, we give a brief review of the model, focusing on its action and symmetries.

The IKKT action consists of a bosonic part and a fermionic part,

$$
\begin{aligned}
S &= S_{\rm b} + S_{\rm f} \ , \\
S_{\rm b} &= -\frac{1}{4g^2}\,{\rm tr}([A_\mu, A_\nu][A^\mu, A^\nu]) \ , \\
S_{\rm f} &= -\frac{1}{2g^2}\,{\rm tr}(\Psi_\alpha\,(C\Gamma^\mu)_{\alpha\beta}[A_\mu, \Psi_\beta]) \ .
\end{aligned}
\tag{6.1}
$$

Here A_μ ($\mu = 0, \ldots, 9$) are $N \times N$ Hermitian matrices. The fermions Ψ_α are Grassmann-valued $N \times N$ matrices in the adjoint representation. After the Weyl projection we have $\alpha = 1, \ldots, 16$ in ten dimensions. The matrices Γ^μ are the ten-dimensional gamma matrices and C is the charge conjugation matrix. The trace is taken over the $N \times N$ matrix indices. Indices are raised and lowered by Lorentzian metric $\eta_{\mu\nu} = {\rm diag}(-1, 1, \ldots, 1)$. With these notations, the action has ${\rm SO}(9,1)$ symmetry.

The model has two supersymmetries, a shift symmetry, and a $U(N)$ gauge symmetry. They can be written as

$$
\begin{aligned}
\delta^{(1)} A_\mu &= i\,\bar\epsilon_1 \Gamma_\mu \Psi \ , \\
\delta^{(1)} \Psi &= \frac{i}{2}\,\Gamma^{\mu\nu}[A_\mu, A_\nu]\,\epsilon_1 \ ,
\end{aligned}
\tag{6.2}
$$

$$
\begin{aligned}
\delta^{(2)} A_\mu &= 0 \ , \\
\delta^{(2)} \Psi &= \epsilon_2\,\mathbf{1}_N \ ,
\end{aligned}
\tag{6.3}
$$

$$
\delta_T A_\mu = c_\mu\,\mathbf{1}_N \ , \qquad \delta_T \Psi = 0 \ ,
\tag{6.4}
$$

$$
\delta_G A_\mu = i[\lambda, A_\mu] \ , \qquad \delta_G \Psi = i[\lambda, \Psi] \ .
\tag{6.5}
$$

Here ϵ_1 and ϵ_2 are ten-dimensional Majorana–Weyl spinors and are Grassmann odd. The parameter c_μ is a real vector, $\mathbf{1}_N$ is the $N \times N$ identity matrix, and λ is an $N \times N$ Hermitian matrix. The transformation (6.5) is the $U(N)$ gauge symmetry after dimensional reduction to zero dimensions. The shift symmetry (6.4) plays the role of translations in the spacetime interpretation as follows.

It is useful to introduce linear combinations of the two supercharges so that the supersymmetry algebra takes the standard form. Let $Q^{(1)}$, $Q^{(2)}$, and P_μ be the generators of (6.2), (6.3), and (6.4), respectively. Define

$$
\begin{aligned}
\tilde{Q}^{(1)} &= Q^{(1)} + Q^{(2)} \ , \\
\tilde{Q}^{(2)} &= i\big(Q^{(1)} - Q^{(2)}\big) \ .
\end{aligned}
\tag{6.6}
$$

Then, up to terms proportional to the gauge transformation (6.5) and to the fermionic equation of motion, one obtains

$$
\big\{\bar\epsilon_1 \tilde{Q}^{(i)}\,,\, \bar\epsilon_2 \tilde{Q}^{(j)}\big\} = -2\,\delta^{ij}\,\bar\epsilon_1 \Gamma^\mu \epsilon_2\,P_\mu \ .
\tag{6.7}
$$

This relation suggests that P_μ acts as a translation generator. Accordingly, the shift symmetry (6.4) supports the interpretation that the eigenvalues of A_μ can be viewed as spacetime coordinates. The model therefore provides a framework in which spacetime can be read off dynamically from matrix degrees of freedom.

As an aside, the connection to perturbative type IIB string theory can be understood from a worldsheet viewpoint. Starting from the Schild-type Green–Schwarz action and applying a matrix regularization,

$$\{\,\cdot\,,\,\cdot\,\} \;\to\; -i[\,\cdot\,,\,\cdot\,]\;, \qquad \frac{1}{2\pi}\int d^2\sigma \;\to\; \mathrm{tr}\;, \tag{6.8}$$

the worldsheet fields X_μ and ψ are mapped to matrices A_μ and Ψ, reproducing the IKKT action. Moreover, the Schild-type Green–Schwarz action describes a *single* string worldsheet, i.e. a first-quantized formulation. In the matrix model, on the other hand, one may consider approximately block-diagonal configurations of the matrices. In such configurations the action is (to a good approximation) written as a sum of the contributions from each block. By applying the correspondence (6.8) to each block, one can associate each block with a Schild-type worldsheet action, and hence interpret the configuration as a multi-string state. In this picture, each string worldsheet may have a different topology. The off-diagonal blocks then naturally represent interactions among different strings. In this sense, the IKKT matrix model is expected to provide a second-quantized description of strings.

In the following, we focus on the Lorentzian IKKT model, which enables dynamical discussions of time evolution within the matrix degrees of freedom. In the next section, we explain how the Lorentzian model is defined at the level of the path integral.

7 Definition of the Lorentzian IKKT model

In this section we define the Lorentzian IKKT model. Unlike the Euclidean model, the Lorentzian partition function is not absolutely convergent and therefore requires some regularization. A definition based on a convergence factor is effectively connected to the Euclidean model through contour deformation. To avoid this, we introduce a Lorentz invariant mass term. Moreover, since the Lorentz symmetry group is noncompact, its treatment in the path integral requires some care. We will explain a practical prescription to handle this issue in the subsections below.

7.1 Equivalence to the Euclidean model

In this subsection, we recall a standard analytic continuation of the Lorentzian IKKT model and explain how it becomes continuously connected to the Euclidean model.

The partition function of the Lorentzian model is formally given by

$$Z = \int dA\, d\Psi\ e^{i(S_{\rm b}+S_{\rm f})}\ . \tag{7.1}$$

Integrating out the fermions gives a Pfaffian,

$$Z = \int dA\ e^{iS_{\rm b}}\ \mathrm{Pf}\,\mathcal{M}(A)\ , \tag{7.2}$$

where $\mathcal{M}$ is an antisymmetric matrix that represents the linear map

$$(\mathcal{M}\Psi)_\alpha = (C\Gamma^\mu)_{\alpha\beta}\,[A_\mu, \Psi_\beta]\ , \tag{7.3}$$

acting on the space of traceless complex $N \times N$ matrices.

A characteristic feature of the Lorentzian formulation is that the bosonic factor is a pure phase, $e^{iS_{\rm b}}$, rather than a positive Boltzmann weight. Because of this oscillatory weight, the matrix integral is not absolutely convergent and thus requires a prescription, which can be implemented by an analytic continuation. To make this more explicit, we introduce

$$F_{\mu\nu} = i[A_\mu, A_\nu]\ . \tag{7.4}$$

With this definition, the bosonic action can be rewritten as

$$S_{\rm b} = \frac{N}{4}\Big\{ -2\,\mathrm{tr}(F_{0i})^2 + \mathrm{tr}(F_{ij})^2 \Big\}\ , \tag{7.5}$$

where $i, j = 1, \ldots, 9$ denote spatial directions. The action (7.5) is real, but it is not positive definite.

A simple way to define the integral is to introduce convergence factors[1]

$$S^{(\varepsilon)} = \frac{N}{4}\left\{-2e^{-i\varepsilon}\,\mathrm{tr}(F_{0i})^2 + e^{i\varepsilon}\,\mathrm{tr}(F_{ij})^2\right\}\ , \tag{7.6}$$

and then take the limit $\varepsilon \to 0^+$.

We next show that this prescription continuously connects the Lorentzian model to the Euclidean model through a contour deformation. Introducing Hermitian matrices $\tilde{A}_\mu$, we rotate the integration contour as [7]

$$A_0 = e^{\frac{i\pi}{8}(s-4k)}\,\tilde{A}_0\ , \qquad A_i = e^{\frac{i\pi}{8}s}\,\tilde{A}_i\ , \tag{7.7}$$

[1]These convergence factors explicitly break SO(9, 1) Lorentz symmetry. Since the Lorentz group is noncompact, the restoration of Lorentz symmetry in the $\varepsilon \to 0^+$ limit is subtle; we return to this point later.

where s and k are real parameters. This defines an analytic continuation of the original Lorentzian integral by integrating over the Hermitian matrices $\tilde{A}_\mu$.

It is convenient to rewrite the phase factor as $e^{iS_{\rm b}} = e^{-\tilde{S}_{\rm b}}$ with $\tilde{S}_{\rm b} \equiv -iS_{\rm b}$. The deformed bosonic action becomes

$$\tilde{S}_{\rm b} = -\frac{i}{4} N\, e^{\frac{i\pi}{2}s} \Big\{ -2\, e^{-i\pi k}\, \mathrm{tr}(\tilde{F}_{0i})^2 + \mathrm{tr}(\tilde{F}_{ij})^2 \Big\} \ , \qquad \tilde{F}_{\mu\nu} = i[\tilde{A}_\mu, \tilde{A}_\nu] \ . \tag{7.8}$$

A particularly useful one-parameter family is obtained by setting $s = k = u$. In that case, the action can be written as

$$\tilde{S}_{\rm b} = \frac{N}{4} \Big[2\, e^{\frac{i\pi}{2}(1-u)}\, \mathrm{tr}(\tilde{F}_{0i})^2 + e^{-\frac{i\pi}{2}(1-u)}\, \mathrm{tr}(\tilde{F}_{ij})^2 \Big] \ . \tag{7.9}$$

For $0 < u \leq 1$, the coefficients in (7.9) have positive real parts, so the bosonic integral is well-defined in this domain. Moreover, for observables that are holomorphic in the matrix variables, expectation values are independent of u within $0 < u \leq 1$ by Cauchy's theorem. In this sense, the Lorentzian limit $u \to 0^+$ and the Euclidean point $u = 1$ are continuously connected within the same definition.

The fermionic Pfaffian is also well behaved under this contour deformation. Under (7.7), the linear map (7.3) is deformed accordingly, and $\mathrm{Pf}\,\mathcal{M}(A)$ is replaced by $\mathrm{Pf}\,\mathcal{M}(e^{-i\pi k/2}\tilde{A}_0, \tilde{A}_i)$ up to an overall phase. Such a phase is irrelevant for normalized expectation values. Since the Pfaffian is a polynomial in A_μ, the contour deformation is well-defined also in the presence of fermions.

7.2 Adding a Lorentz invariant mass term

The definition above makes the Lorentzian model smoothly connected to the Euclidean model through the deformation parameter. If one aims instead at a definition that is not tied to this Lorentzian–Euclidean equivalence, and in particular at an emergent spacetime that is genuinely Lorentzian in the usual sense, it is natural to consider an alternative regularization. Following Refs. [8–10], we introduce a Lorentz invariant mass term

$$S_{\rm m} = -\frac{1}{2}\, N\gamma\ \mathrm{tr}(A_\mu A^\mu) = \frac{1}{2}\, N\gamma \left\{ \mathrm{tr}\big(A_0^2\big) - \mathrm{tr}\big(A_i^2\big) \right\} \ , \tag{7.10}$$

where the coefficient γ is real.

When the mass term is present, it is convenient to introduce the convergence factor directly in the mass term and define

$$S_{\rm m}^{(\varepsilon)} = \frac{1}{2}\, N\gamma \left\{ e^{i\varepsilon}\, \mathrm{tr}\big(A_0^2\big) - e^{-i\varepsilon}\, \mathrm{tr}\big(A_i^2\big) \right\} \ . \tag{7.11}$$

We then define the theory by taking $\varepsilon \to 0^+$ for $\gamma > 0$, and $\varepsilon \to 0^-$ for $\gamma < 0$, assuming that the limit is taken at finite N and finite γ.

With the mass term (7.11) added to the original Lorentzian action, the bosonic partition function is replaced by

$$Z = \int \mathrm{d}A \, e^{iS} \ , \tag{7.12}$$

$$S = -\frac{N}{4} \operatorname{tr}([A_\mu, A_\nu][A^\mu, A^\nu]) + \frac{1}{2} N\gamma \left\{ e^{i\varepsilon} \operatorname{tr}\left(A_0^2\right) - e^{-i\varepsilon} \operatorname{tr}\left(A_i^2\right) \right\} \ . \tag{7.13}$$

It is instructive to compare this with the Euclidean definition by formally applying the same contour deformation (7.7) at $u = 1$ (i.e. $s = k = 1$). One then obtains a Boltzmann weight $e^{-\tilde{S}}$ with the action

$$\tilde{S} = \frac{N}{4} \left\{ 2 \operatorname{tr}\left(\tilde{F}_{0i}\right)^2 + \operatorname{tr}\left(\tilde{F}_{ij}\right)^2 \right\} + \frac{1}{2} N\gamma \, e^{3\pi i/4} \left\{ \operatorname{tr}\left(\tilde{A}_0^2\right) + \operatorname{tr}\left(\tilde{A}_i^2\right) \right\} \ . \tag{7.14}$$

For $\gamma < 0$, the mass term in (7.14) is bounded below. Therefore the resulting model is smoothly connected to the Euclidean IKKT model in the limit $\gamma \to 0^-$. For $\gamma > 0$, however, the situation changes qualitatively. In this case the mass term in (7.14) is unbounded below, so the same contour deformation is no longer admissible. This is precisely why we introduce the Lorentz invariant mass term with $\gamma > 0$ in (7.11), which allows us to define the Lorentzian model in a way that is not continuously connected to the Euclidean theory, and hence to pursue a definition that is genuinely Lorentzian.

The mass term also has an important consequence at the classical level. The classical equation of motion obtained from the IKKT action supplemented by (7.10) reads

$$[A^\nu, [A_\nu, A_\mu]] - \gamma A_\mu = 0 \ . \tag{7.15}$$

For $\gamma > 0$, this equation admits classical solutions that describe a real, smooth, and expanding spacetime. For $\gamma = 0$, classical solutions consist only of simultaneously diagonalizable configurations of A_μ [11], and hence there is no classical mechanism for spacetime expansion. For $\gamma < 0$, the only classical solution is the trivial one $A_\mu = 0$.

However, the existence of expanding solutions for $\gamma > 0$ does not by itself determine the dimensionality of the expanding space. Indeed, classical expanding solutions can be found with various dimensionalities, so a specific dimensionality cannot be selected at the classical level alone.

The selection is expected to arise from quantum fluctuations. Such effects become increasingly important as γ is decreased, which is the regime relevant for approaching the massless limit after taking the large-N limit. For this reason, in the following we study the model by numerical simulations in order to incorporate quantum effects and to investigate which dimensionality is selected dynamically.

7.3 "Gauge-fixing" the Lorentz symmetry

A central difficulty of the Lorentzian IKKT matrix model is that the Lorentz group is noncompact. This noncompactness has a direct impact on the path integral and can lead to divergences associated with the boost directions [12].

Both the action and the integration measure are $\mathrm{SO}(9,1)$ Lorentz invariant. Therefore, if a configuration A_μ contributes to the partition function, then any Lorentz transformed configuration contributes with the same weight. In particular, Lorentz boosts generate infinitely many configurations that belong to the same Lorentz orbit. As a result, the integral can contain an infinite volume coming from the boost directions. This is the basic reason why the partition function can diverge around nontrivial saddle points: all boosted versions of the same saddle point contribute with the same weight, so the integral over the boost parameters is not finite.

A conventional way to make the oscillatory integral well-defined is to introduce a small convergence factor and remove it at the end. In the purely bosonic model, this can be implemented by modifying the action as in Eq. (7.6) and taking the limit $\varepsilon \to +0$ after the integration. If the Lorentz invariant mass term is included, one may instead introduce the convergence factor directly in the mass term as in Eq. (7.11). In either implementation the integral is convergent at finite ε. However, the cutoff breaks $\mathrm{SO}(9,1)$ explicitly, and the resulting cutoff artifact can persist even in the $\varepsilon \to 0$ limit because the Lorentz group is noncompact.

These observations motivate a different strategy. Instead of regulating the divergent boost volume by an explicit symmetry-breaking cutoff, we remove the boost volume from the beginning while keeping the Lorentz symmetry of the model. For this purpose we implement a "gauge-fixing" of the Lorentz symmetry directly in the path integral. The underlying idea is analogous to removing zero modes in perturbation theory, but here we impose it nonperturbatively.

We choose a representative Lorentz frame by minimizing $\mathrm{tr}(A_0)^2$. Consider a boost that mixes A_0 with one spatial matrix A_j. If a configuration A_μ is already at the minimum of $\mathrm{tr}(A_0)^2$, the first derivative of $\mathrm{tr}(A_0)^2$ with respect to the boost parameter must vanish at zero boost. This condition implies

$$\mathrm{tr}(A_0 A_i) = 0 \qquad (i = 1, \ldots, 9) \ . \tag{7.16}$$

Conversely, if (7.16) holds, any finite boost increases $\mathrm{tr}(A_0)^2$, which shows that (7.16) is equivalent to selecting the frame that minimizes $\mathrm{tr}(A_0)^2$.

We fix the Lorentz boosts by the Faddeev–Popov procedure. We insert

$$1 = \int d\omega\, \Delta_{\rm FP}(A^{(\omega)}) \prod_{i=1}^{9} \delta\Big(\mathrm{tr}(A_0^{(\omega)} A_i^{(\omega)})\Big) \tag{7.17}$$

into the original path integral, and factor out the divergent boost volume $\int d\omega$. As a result, we define the gauge-fixed partition function by

$$Z_{\rm gf} = \int dA\, e^{iS[A]}\, \Delta_{\rm FP}[A] \prod_{i=1}^{9} \delta(\mathrm{tr}(A_0 A_i)) \ . \tag{7.18}$$

For the gauge condition (7.16), the Faddeev–Popov factor can be written as

$$\Delta_{\rm FP}[A] = \det \Omega \ , \tag{7.19}$$

with

$$\Omega_{ij} = \mathrm{tr}(A_0)^2\, \delta_{ij} + \mathrm{tr}(A_i A_j) \ . \tag{7.20}$$

This gauge fixing removes the noncompact boost directions. The remaining integral is over one representative configuration on each Lorentz orbit, and hence the divergent boost volume no longer appears. A convergence factor can still be introduced when needed to make the integral absolutely convergent. The crucial point is that the gauge-fixed formulation eliminates the noncompact flat directions associated with Lorentz boosts, and therefore it can avoid the severe cutoff artifact that arises in the conventional ε regularization.

In practice, the gauge-fixing constraints are implemented by adding a sharply peaked term $S_{\rm g.f.}$ to the effective action; see App. C.

8 Complex Langevin method

In this section we summarize the complex Langevin method (CLM) and explain how we apply it to the Lorentzian IKKT matrix model. The CLM is a stochastic approach to path integrals with complex weights, in which the dynamical variables are complexified and evolved in a fictitious Langevin time. For the IKKT model, this provides a practical framework to study the oscillatory Lorentzian weight and to incorporate quantum fluctuations numerically.

We first introduce the time coordinate and a set of observables used to characterize the spatial structure extracted from matrix configurations (Sec. 8.1). We then review the general formulation of the CLM (Sec. 8.2) and explain how the time ordering in the diagonal gauge of A_0 is implemented after complexification, leading to an effective action suitable for

the CLM evolution (Sec. 8.3). We also describe how observables that are non-holomorphic at the level of eigenvalues are treated in a holomorphically consistent manner within the CLM.

8.1 Time coordinate and observables for spatial structure

In the IKKT model, spacetime does not exist *a priori*. We define a notion of time and observables for spatial structure from the matrix degrees of freedom. We fix an SU(N) gauge in which the temporal matrix A_0 is diagonal and order its eigenvalues as

$$A_0 = \mathrm{diag}(\alpha_1, \alpha_2, \ldots, \alpha_N), \qquad \alpha_1 \leq \alpha_2 \leq \cdots \leq \alpha_N. \tag{8.1}$$

From the ordered eigenvalues $\{\alpha_a\}$ we define a time coordinate as an observable constructed from A_0 in the diagonal gauge. Fix an integer n (the block size) and introduce the averaged eigenvalues

$$\bar{\alpha}_{k+1} = \frac{1}{n}\sum_{\nu=1}^{n} \alpha_{k+\nu}, \qquad (k = 0, 1, \ldots, N-n), \tag{8.2}$$

and define

$$t_0 = 0, \qquad t_k = \sum_{b=1}^{k} \left|\bar{\alpha}_{b+1} - \bar{\alpha}_b\right|, \qquad (k = 1, 2, \ldots, N-n). \tag{8.3}$$

In this basis, the spatial matrices A_i obtained in the CLM typically exhibit an approximate band-diagonal structure. More precisely, for a suitable choice of n, the matrix elements $(A_i)_{ab}$ with $|a-b| > n$ are much smaller in magnitude than those with $|a-b| \leq n$ in typical configurations. To visualize and quantify this structure, we consider

$$\mathcal{A}_{ab} = \frac{1}{9}\sum_{i=1}^{9} \left|(A_i)_{ab}\right|^2, \qquad (a, b = 1, 2, \ldots, N). \tag{8.4}$$

Motivated by the observed band-diagonal structure, we introduce the $n \times n$ block matrices $\bar{A}_i(t_k)$ by

$$\left(\bar{A}_i(t_k)\right)_{pq} = (A_i)_{k+p,\,k+q}, \qquad (p, q = 1, 2, \ldots, n), \tag{8.5}$$

where $k = 0, 1, \ldots, N-n$ labels the block associated with t_k.

Using the block matrices $\bar{A}_i(t_k)$ defined above, we introduce observables that characterize the spatial extent and its anisotropy. We define the extent of space at time t_k by

$$R^2(t_k) = \left\langle \frac{1}{n}\,\mathrm{tr}\sum_{i=1}^{9}\left(\bar{A}_i(t_k)\right)^2 \right\rangle = e^{2i\theta_s(t_k)}\left|R^2(t_k)\right|, \tag{8.6}$$

where tr denotes the trace over the $n \times n$ block. The phase $\theta_s(t_k)$ monitors whether $R^2(t_k)$ is approximately real or exhibits a fixed phase rotation; in particular, $\theta_s(t_k) \simeq 0$ indicates an approximately real extent, while $\theta_s(t_k) \simeq \pi/8$ corresponds to the Euclidean-type phase rotation in the analytic continuation.

To probe possible anisotropy, we define the 9×9 moment of inertia tensor

$$T_{ij}(t_k) = \frac{1}{n} \operatorname{tr}\big(\bar{A}_i(t_k)\, \bar{A}_j(t_k)\big)\,, \qquad (i,j = 1,\dots,9). \tag{8.7}$$

We diagonalize $T(t_k)$ as

$$U(t_k)^{-1} T(t_k)\, U(t_k) = \operatorname{diag}\big(\lambda_1(t_k), \lambda_2(t_k), \dots, \lambda_9(t_k)\big), \tag{8.8}$$

and order the eigenvalues by $\operatorname{Re}\lambda_1(t_k) \geq \cdots \geq \operatorname{Re}\lambda_9(t_k)$. By construction,

$$\sum_{i=1}^{9} \lambda_i(t_k) = \frac{1}{n} \operatorname{tr} \sum_{i=1}^{9} \big(\bar{A}_i(t_k)\big)^2, \tag{8.9}$$

so $\sum_{i=1}^{9} \langle \lambda_i(t_k) \rangle = R^2(t_k)$. If $\operatorname{Re}\langle\lambda_1(t_k)\rangle, \dots, \operatorname{Re}\langle\lambda_d(t_k)\rangle$ become larger than the rest, this indicates spontaneous symmetry breaking $\mathrm{SO}(9) \to \mathrm{SO}(d)$ and the dynamical selection of an effectively d-dimensional spatial structure.

To further probe the spatial distribution, we consider the $n \times n$ matrix [13]

$$Q(t_k) = \sum_{i=1}^{9} \big(\bar{A}_i(t_k)\big)^2. \tag{8.10}$$

For Hermitian $\bar{A}_i(t_k)$, the eigenvalues of $Q(t_k)$ provide the radial distribution of points in space.

In the CLM, the ordering in (8.1) is implemented holomorphically by introducing auxiliary variables τ_a, and effective eigenvalues of $T(t_k)$ are extracted from holomorphic observables; see Sec. 8.3.

We have thus defined a time coordinate and a set of observables that characterize the spatial extent and its symmetry breaking pattern. In the following subsections, we explain how these quantities are evaluated using the complex Langevin method [14, 15].

8.2 General formulation

To describe the CLM in general terms, let us consider a model with real variables $x = (x_1, \dots, x_n) \in M$ and a complex weight $w(x)$, so that the partition function is

$$Z = \int_M dx\; w(x)\;, \tag{8.11}$$

where M denotes the manifold of the original real variables. It is often convenient to write $w(x) = e^{-S(x)}$ with a complex action $S(x)$.

In the CLM one complexifies the variables, $x \to z$, and regards $z = (z_1, \ldots, z_n)$ as coordinates on the complexified manifold $M^{\mathbb{C}}$. Writing $z_k = x_k + iy_k$, the dynamics is defined by the complex Langevin equation

$$\frac{dz_k}{d\sigma} = \frac{\partial}{\partial z_k} \log w(z) + \eta_k(\sigma) = -\frac{\partial S(z)}{\partial z_k} + \eta_k(\sigma) \ , \tag{8.12}$$

where the first term is the drift term. The noise $\eta_k(\sigma)$ is taken to be real Gaussian noise, characterized for instance by

$$\exp\left(-\frac{1}{4} \int d\sigma \sum_{k=1}^{n} \eta_k(\sigma)^2 \right) \ , \tag{8.13}$$

equivalently $\langle \eta_k(\sigma) \eta_\ell(\sigma') \rangle = 2\, \delta_{k\ell} \delta(\sigma - \sigma')$.

The Langevin process defines a probability distribution $P(x, y; \sigma)$ on the real variables (x, y) of the complexified manifold, which satisfies a (real) Fokker–Planck equation associated with (8.12). If the process converges, $P(x, y; \sigma)$ approaches a stationary distribution $P(x, y)$ as $\sigma \to \infty$. For an observable $\mathcal{O}[x]$, one compares the original expectation value with the one computed in the complexified formulation. If the relation

$$\int dx\, dy\ \mathcal{O}(x + iy)\ P(x, y) = \int_M dx\ \mathcal{O}(x)\ w(x) \tag{8.14}$$

holds, the expectation value can be evaluated as an average along the Langevin trajectory,

$$\langle \mathcal{O}[x] \rangle = \lim_{\sigma \to \infty} \frac{1}{\sigma} \int_{\sigma_0}^{\sigma_0 + \sigma} d\sigma'\ \mathcal{O}[z(\sigma')] \ , \tag{8.15}$$

where σ_0 denotes a Langevin time after which the evolution has reached equilibrium. In practice, holomorphy of both the complex weight $w(z)$ and the observable $\mathcal{O}(z)$ is essential in the standard justification of (8.14) and (8.15).

In the following, we apply the CLM to the Lorentzian IKKT model. We first explain how the ordering of the eigenvalues of A_0 is implemented after complexification and how the corresponding contributions are incorporated into an effective action S_{eff} (Sec. 8.3). We then discuss how observables that are non-holomorphic at the level of eigenvalues are evaluated in a holomorphically consistent way.

8.3 Time ordering and the effective action

We now explain how the time ordering introduced in (8.1) is implemented in the CLM and how the corresponding effective action is obtained. After complexification, the eigenvalues

α_a of A_0 become complex, so the notion of ordering has to be incorporated in a holomorphically consistent parametrization. Following Ref. [16], we introduce auxiliary variables τ_a $(a = 1, \ldots, N-1)$ and parameterize the eigenvalues as

$$\alpha_1 = 0 \ , \qquad \alpha_k = \sum_{i=1}^{k-1} e^{\tau_i} \qquad (k = 2, \ldots, N) \ . \tag{8.16}$$

For real τ_a, this parametrization enforces $\alpha_1 \le \alpha_2 \le \cdots \le \alpha_N$, and it also provides a smooth extension after complexification.

Diagonalizing A_0 produces the Vandermonde determinant for the eigenvalues, and the change of variables (8.16) yields an additional Jacobian factor. Together, these contributions appear as an additive term in the effective action,

$$S_{A\mathrm{diag}} = -\log \prod_{1 \le a < b \le N} (\alpha_a - \alpha_b)^2 - \sum_{a=1}^{N-1} \tau_a \ . \tag{8.17}$$

With these ingredients, the effective partition function investigated by the CLM is written as

$$\begin{aligned} Z_{\mathrm{eff}} &= \int dA_i \, d\tau \ e^{-S_{\mathrm{eff}}} \ , \\ S_{\mathrm{eff}} &= -i\big(S_{\mathrm{b}} + S_{\mathrm{m}}\big) + S_{A\mathrm{diag}} + S_{\mathrm{g.f.}} - \log \mathrm{Pf}\, \mathcal{M} \ . \end{aligned} \tag{8.18}$$

where S_{b}, S_{m} and $S_{\mathrm{g.f.}}$ are given in Eqs. (7.5), (7.10) and (C.8), respectively, and $\mathcal{M}$ is the antisymmetric fermion matrix defined in Eq. (7.3).

In the CLM, we complexify τ_a and A_i and evolve them in a fictitious Langevin time σ. The complex Langevin equations read

$$\frac{d\tau_a}{d\sigma} = -\frac{\partial S_{\mathrm{eff}}}{\partial \tau_a} + \eta_a(\sigma) \ , \qquad \frac{d(A_i)_{ab}}{d\sigma} = -\frac{\partial S_{\mathrm{eff}}}{\partial (A_i)_{ba}} + (\eta_i)_{ab}(\sigma) \ , \tag{8.19}$$

where $\eta_a(\sigma)$ are real Gaussian noises and $(\eta_i)_{ab}(\sigma)$ are Hermitian-matrix Gaussian noises, drawn from probability distributions proportional to

$$\exp\left(-\frac{1}{4}\int d\sigma \sum_a \eta_a(\sigma)^2\right), \qquad \exp\left(-\frac{1}{4}\int d\sigma \ \mathrm{tr}\ \eta_i(\sigma)^2\right), \tag{8.20}$$

respectively. In the supersymmetric model, the Pfaffian term can induce exceptionally large drifts when $\mathcal{M}$ develops near-zero modes; we return to this singular-drift issue later in Sec. 9.2.

Finally, we explain how we treat observables that are not holomorphic after complexification. In the CLM, the 9×9 matrix $T(t_k)$ introduced in Sec. 8.1 becomes non-Hermitian

in general, and its eigenvalues $\lambda_i(t_k)$ are not holomorphic functions of the complexified variables. Therefore, we do not use $\langle \lambda_i(t_k) \rangle$ obtained by a naive diagonalization. Instead, we consider the characteristic polynomial

$$\det(z\,\mathbf{1}_9 - T(t_k)) = \sum_{\ell=0}^{9} c_\ell(t_k)\, z^\ell, \tag{8.21}$$

where the coefficients $c_\ell(t_k)$ are polynomials in the components of $T(t_k)$ and hence holomorphic functions of the complexified variables. We therefore compute $\langle c_\ell(t_k) \rangle$ reliably within the CLM and solve

$$\sum_{\ell=0}^{9} \langle c_\ell(t_k) \rangle\, z^\ell = 0 \tag{8.22}$$

to define effective eigenvalues as the roots $z_i(t_k)$ of (8.22), labeled so that $\mathrm{Re}\, z_1(t_k) \geq \cdots \geq \mathrm{Re}\, z_9(t_k)$. Error bars are estimated using the jackknife method.

9 Results of complex Langevin simulations

In this section we present the results of complex Langevin simulations for the deformed Lorentzian IKKT matrix model studied in this work. We first discuss the bosonic model, in which the Pfaffian is replaced by a constant, and then turn to the model including the fermionic contribution. Unless stated otherwise, we use the block size n and the definition of time and observables introduced in Sec. 8.1.

9.1 Bosonic model

We first consider the bosonic model, in which the Pfaffian is replaced by a constant. Using the block variables $\bar{A}_i(t_k)$ and the observables defined in Sec. 8.1, we examine the reality of the time coordinate and the possible anisotropy of the spatial extent.

Figure 6 shows representative results. In the late-time region, the expectation values $\langle \alpha_a \rangle$ lie close to the real axis in the complex plane, indicating that the time coordinate constructed from A_0 is approximately real in that region. In addition, the nine eigenvalues of $T_{ij}(t)$ are nearly degenerate (see Sec. 8.3), which indicates that no spontaneous breaking of the spatial SO(9) symmetry is observed in this parameter set.

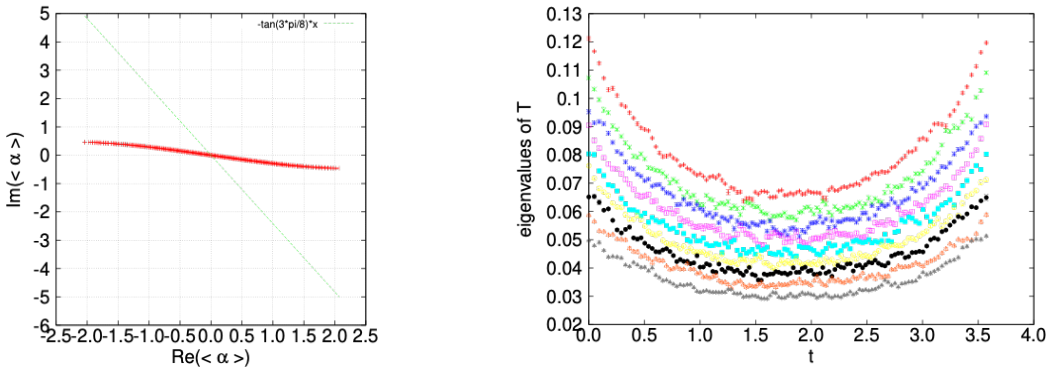

Figure 6: Bosonic model with $N = 128$ and $\gamma = 4$. (Left) Expectation values $\langle \alpha_a \rangle$ of the eigenvalues of the temporal matrix A_0 in the complex plane. (Right) Real parts of the eigenvalues of $T_{ij}(t)$.

9.2 Model including fermions

We now turn to simulations including the fermionic contribution. As mentioned in Sec. 8.3, the Pfaffian term in the effective action can induce exceptionally large drifts when the fermion matrix $\mathcal{M}(A)$ develops near-zero modes. This singular-drift problem [17–19] is reflected in the Pfaffian contribution to the drift,

$$\frac{\partial}{\partial (A_i)_{ba}} \Big\{ - \log \mathrm{Pf}\, \mathcal{M} \Big\} = -\frac{1}{2} \,\mathrm{tr} \left(\frac{\partial \mathcal{M}}{\partial (A_i)_{ba}} \, \mathcal{M}^{-1} \right) , \tag{9.1}$$

which becomes large when $\mathcal{M}$ develops near-zero modes.

Following Refs. [20, 21], we introduce a fermionic mass term m_{f},

$$S_{m_{\mathrm{f}}} = -\frac{N}{2} \, i m_{\mathrm{f}} \,\mathrm{tr}\, \bar{\Psi} \big(\Gamma^7 (\Gamma^8)^\dagger \Gamma^9 \big) \Psi \, . \tag{9.2}$$

For real m_{f}, this term shifts the spectrum of $\mathcal{M}(A)$ away from the origin and suppresses the appearance of exceptionally large drifts. For large m_{f} the fermions effectively decouple and the model approaches the bosonic one, whereas for smaller m_{f} fermionic effects become more pronounced but the singular drift problem becomes more severe.

To enhance fermionic effects while keeping the CLM reliable, we also introduce an anisotropic deformation of the mass term (7.10),

$$S_\gamma = \frac{1}{2} N \gamma \left(\mathrm{tr}\big(A_0^2\big) - \sum_{i=1}^{\tilde{d}} \mathrm{tr}\big(A_i^2\big) - \xi \sum_{j=\tilde{d}+1}^{9} \mathrm{tr}\big(A_j^2\big) \right) \, . \tag{9.3}$$

This deformation explicitly distinguishes the first $\tilde{d}$ spatial directions from the remaining ones. In the following, we investigate the time-dependent observables defined in Sec. 8.1

and study the late-time behavior of the spatial extent and its anisotropy. Unless stated otherwise, we use the parameter set

$$N = 128\,, \qquad n = 6\,, \qquad \gamma = 4\,, \qquad m_{\rm f} = 5\,, \qquad \tilde{d} = 5\,, \qquad \xi = 10\,. \tag{9.4}$$

9.2.1 Band–diagonal structure of spatial matrices

We first check the band-diagonal structure assumed in Sec. 8.1 by measuring $\mathcal{A}_{ab}$ defined in Eq. (8.4). Figure 7 shows $\mathcal{A}_{ab}$ for the parameter set (9.4). We observe that $\mathcal{A}_{ab}$ is strongly localized near $a = b$ and rapidly decreases as $|a - b|$ increases, which supports the use of the block variables $\bar{A}_i(t_k)$ defined in (8.5).

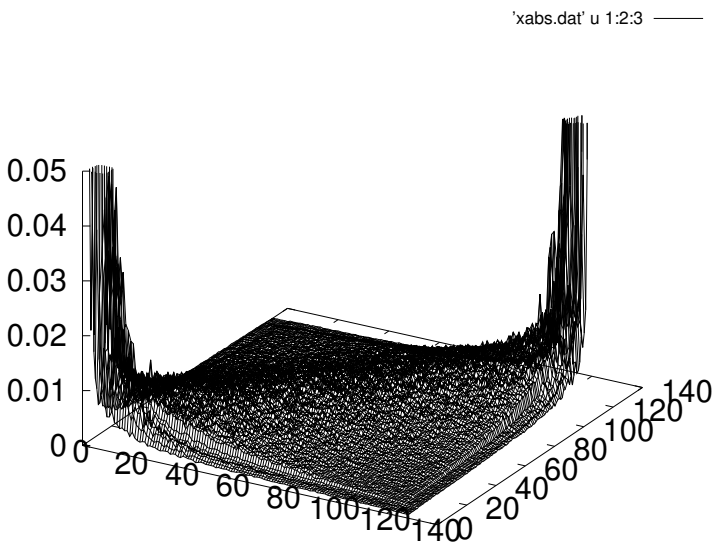

Figure 7: Band–diagonal structure of the spatial matrices visualized by $\mathcal{A}_{ab}$ for the parameter set (9.4). The height represents $\mathcal{A}_{ab}$, which is strongly localized near $a = b$.

Figure 8 shows $\langle \alpha_a \rangle$ in the complex plane. At late times the distribution becomes almost parallel to the real axis, indicating that the time coordinate constructed from A_0 is approximately real also in the fermionic case.

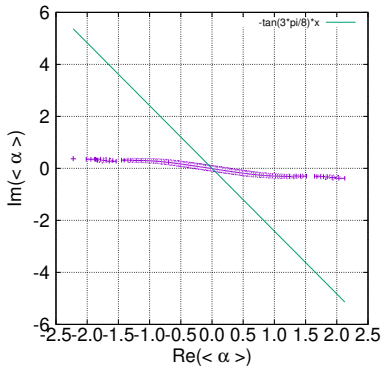

Figure 8: Expectation values of the eigenvalues α_a of A_0 in the complex plane for the parameter set (9.4). At late times the distribution becomes almost parallel to the real axis.

9.2.2 Reality and expansion of the spatial extent

We next examine the phase $\theta_s(t)$ and the spatial extent $R^2(t)$ defined in Eq. (8.6). Figure 9 (Left) shows $\theta_s(t)$ as a function of t. We find that $\theta_s(t)$ stays close to zero throughout the whole time range we have explored, indicating that $R^2(t)$ remains almost real for all t in this parameter set. Figure 9 (Right) shows $\mathrm{Re}\, R^2(t)$ for the same parameter set. We observe that $\mathrm{Re}\, R^2(t)$ starts to grow at late times, while it remains nearly constant at earlier times.

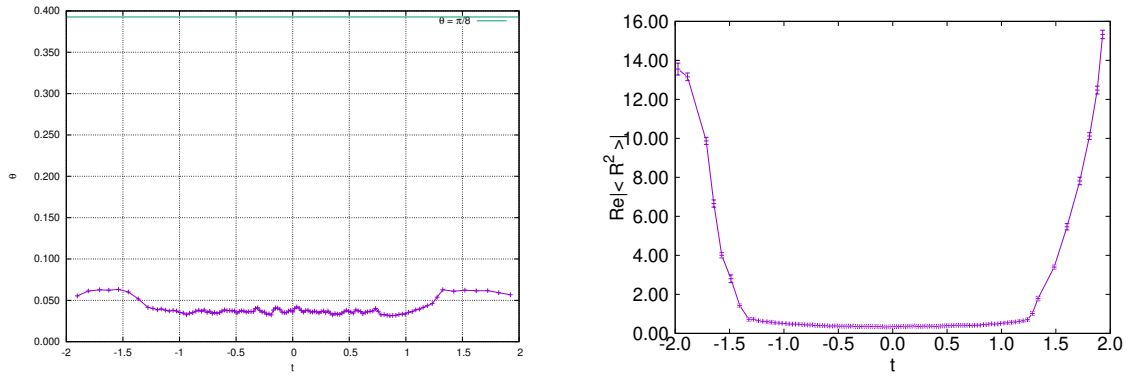

Figure 9: (Left) Phase $\theta_s(t)$ of $R^2(t)$. (Right) Real part $\mathrm{Re}\, R^2(t)$.

9.2.3 Emergence of a $(3+1)$-dimensional expanding spacetime

To explore which dimensionality is selected dynamically from the original ten-dimensional degrees of freedom, we study the moment of inertia tensor $T_{ij}(t)$ defined in Eq. (8.7). Figure 10 shows the real parts of its eigenvalues as functions of t for the parameter set (9.4). At late times, three eigenvalues grow whereas the remaining ones stay small. This indicates that three spatial directions become dominant dynamically at late times.

In the present setup (9.3) with $\tilde{d} = 5$, the deformation explicitly distinguishes the first $\tilde{d}$ spatial directions from the remaining ones. Within this distinguished sector, the observed behavior suggests that three directions become dominant at late times.

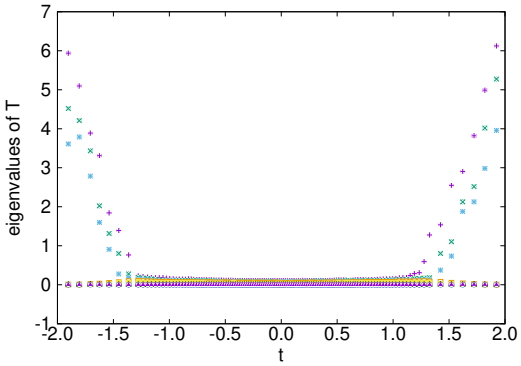

Figure 10: Real parts of the eigenvalues of $T_{ij}(t)$ as functions of time t_k for the parameter set (9.4).

10 Summary and discussion

This thesis investigates real-time quantum dynamics within the path-integral framework in two complementary settings: environment-induced quantum decoherence in many-body quantum mechanics and the extraction of time-dependent spacetime observables in the Lorentzian IKKT matrix model. The common motivation is that a direct Schrödinger-picture treatment of real-time evolution becomes exponentially costly as the number of degrees of freedom grows, while the path-integral representation offers a principled alternative once one exploits its structural features—in particular, the role of complex saddle points in organizing oscillatory real-time integrals, and the reduction to finite-dimensional Gaussian integrals in quadratic models.

Part I: Quantum decoherence from complex saddles

In Part I, we investigated environment-induced decoherence in a closed-system real-time path-integral formulation. The central idea was to regard the reduced density matrix not as the solution of an approximate master equation, but as an object characterized directly by a complex saddle point of the discretized effective action. As a standard benchmark, we first reviewed the Caldeira–Leggett (CL) model and summarized two complementary viewpoints: the conventional continuum master-equation description in the Ohmic high-

temperature limit, and an exact closed-system path-integral formulation in which the total system evolves unitarily and the environment is traced out only at the final time.

In the latter formulation, real time was discretized and the thermal initial state of the environment was represented by an additional imaginary-time path. For Gaussian initial conditions, the resulting effective action is quadratic in all integration variables, so that the reduced density matrix can be evaluated exactly by a Gaussian saddle-point calculation. This leads to an explicit Gaussian form of the reduced density matrix, from which we extracted decoherence diagnostics by parametrizing the real part of the exponent in terms of two coefficients J and K and defining the diagonal and off-diagonal damping rates $\Gamma_{\text{diag}}(t)$ and $\Gamma_{\text{off-diag}}(t)$. Within this framework, the CL model provides a benchmark for the early-time behavior of $\Gamma_{\text{off-diag}}(t)$.

Motivated by this benchmark, we then turned to a three-dimensional cubic lattice toy model intended to mimic a large molecule. Within a single closed model at the level of the action, we separated the degrees of freedom into center-of-mass (CM) and relative coordinates, treating the CM mode as the subsystem and the relative modes as an effective environment-like sector. A pinning interaction introduces a coupling between the CM mode and the internal sector, and at the same time induces a renormalized CM frequency $\omega_r(c)$ determined by the pinning parameter c. Using this renormalized frequency, we prepared the initial CM state as a Gaussian wave packet, while the relative modes were taken to be in thermal equilibrium at inverse temperature β.

We then evaluated the reduced density matrix of the CM mode and demonstrated a rapid suppression of off-diagonal components in the position basis. This provides a direct numerical manifestation of decoherence in a fully unitary closed system. To quantify this behavior, we extracted $\Gamma_{\text{off-diag}}(t)$ from the Gaussian form of the reduced density matrix and studied its dependence on the pinning coupling c and the inverse temperature β. The off-diagonal suppression becomes stronger for larger c and smaller β.

To examine the early-time behavior more quantitatively, we introduced the rescaled quantity

$$\tilde{\Gamma}(t) = \frac{\beta}{c} \left\{ \Gamma_{\text{off-diag}}(t) - \Gamma_{\text{off-diag}}(0) \right\},$$

and fitted $\Gamma_{\text{off-diag}}(t)$ by a linear function in the time interval where the data are well approximated by a straight line. The two complementary analyses—fixed c with varying β, and fixed β with varying c—yielded mutually consistent results, leading to the representative coefficient

$$A \simeq 6.60 \times 10^{-2} \,. \tag{10.1}$$

Thus, in the parameter region where the linear regime is observed, our numerical results

support the scaling form

$$\Gamma_{\text{off-diag}}(t) \simeq A\,\frac{c}{\beta}\,t + B. \tag{10.2}$$

A notable outcome is that this coupling dependence differs from the CL benchmark. In the CL model, the early-time behavior is governed by the effective damping parameter γ_{CL}, and in the uniform-coupling realization reviewed in this thesis one has $\gamma_{CL} \propto c_{\text{CL}}^2$ for fixed $(\omega_{\text{cut}}, N_{\mathcal{E}})$, which implies $\Gamma_{\text{off-diag}}(t) \propto (c_{\text{CL}}^2/\beta)\,t$ at high temperature. By contrast, in the molecular toy model studied here we observe the scaling $\Gamma_{\text{off-diag}}(t) \propto (c/\beta)\,t$ in the regime analyzed numerically. This difference suggests that decoherence in a composite system with many internal degrees of freedom can exhibit a qualitatively different dependence on the microscopic coupling parameter from that in a point-like system coupled to an external bath. From this point of view, the present result may be interpreted as a characteristic feature of the molecular setting modeled here, and it motivates further investigation of decoherence specific to large molecules.

Part II: Lorentzian IKKT matrix model and spacetime from matrices

In this part we investigated the Lorentzian IKKT matrix model as a nonperturbative formulation of type IIB superstring theory, focusing on how a notion of time and spatial structure can be extracted from matrix configurations. We first reviewed the standard definition of the Lorentzian partition function and explained why, with a conventional convergence prescription, the Lorentzian model can become continuously connected to the Euclidean model through a contour deformation, leading to observables that exhibit a Euclidean-type phase rotation. In order to formulate a model that is not tied to this Lorentzian–Euclidean equivalence, we introduced a Lorentz invariant mass term with parameter γ. For $\gamma > 0$ the same Wick-rotation route was obstructed, and the classical equations of motion admitted nontrivial expanding solutions, which motivated us to investigate quantum effects by numerical simulations.

A key obstacle in the Lorentzian formulation was the noncompactness of the Lorentz group, which could generate a divergent boost volume in the path integral. To remove this divergence without explicitly breaking Lorentz symmetry, we implemented a nonperturbative "gauge-fixing" of Lorentz boosts. We selected a representative frame by minimizing $\mathrm{tr}(A_0^2)$, which led to the condition $\mathrm{tr}(A_0 A_i) = 0$ $(i = 1, \ldots, 9)$, and we derived the corresponding Faddeev–Popov determinant. For practical simulations we reformulated the gauge-fixed partition function by exponentiating the determinant and implementing the

constraint with a sharply peaked term and auxiliary variables, as summarized in Sec. 7.3 and detailed in App. C.

We then applied the complex Langevin method (CLM) to the resulting gauge-fixed Lorentzian matrix integral. After fixing the diagonal gauge for A_0, we parameterized the ordered eigenvalues holomorphically by introducing τ_a variables, which allowed us to define a time coordinate t from the averaged eigenvalues of A_0. Using the observed band-diagonal structure of the spatial matrices in this basis, we constructed block variables $\bar{A}_i(t)$ and evaluated time-dependent observables for the spatial geometry, including the spatial extent $R^2(t)$, its phase diagnostic $\theta_s(t)$, and the moment of inertia tensor $T_{ij}(t)$. Since $T_{ij}(t)$ became non-Hermitian after complexification, we treated its eigenvalues through holomorphic quantities based on the characteristic polynomial, following Sec. 8.3, so that the analysis remained consistent with the holomorphy requirements of the CLM.

We presented CLM results first for the bosonic model (with the Pfaffian replaced by a constant). In this bosonic case, we found that the time coordinate extracted from A_0 is approximately real at late times, while no spontaneous breaking of the spatial SO(9) symmetry was observed for the parameter set studied.

We then included fermions, where the Pfaffian term could induce the singular-drift problem when the fermion matrix $\mathcal{M}(A)$ developed near-zero modes. To regulate this while keeping fermionic effects visible, we introduced a fermionic mass term m_{f} and, in addition, an anisotropic deformation of the mass term. For a representative parameter set we verified the band-diagonal structure, found that the spatial extent remained almost real (with $\theta_s(t)$ staying close to zero), and observed a late-time expansion. Moreover, the eigenvalues of $T_{ij}(t)$ showed that three directions became dominant at late times. In the present setup, where the deformation explicitly distinguishes the first $\tilde{d}$ spatial directions from the remaining ones, this behavior suggests the emergence of a real, expanding $(3+1)$-dimensional spacetime in the gauge-fixed Lorentzian IKKT model with fermions (Sec. 9).

Finally, we emphasized the intended continuum approach: we took the large-N limit first and then explored the behavior as $\gamma \to 0$ and $m_{\mathrm{f}} \to 0$ after establishing numerical control of the CLM.

As a further direction, it is interesting to study a class of deformations of the type IIB matrix model that preserve 16 supercharges, obtained by combining bosonic and fermionic mass terms with a Myers term (App. D). Although this supersymmetry-preserving formulation and the deformation used in the present work are distinct at finite values of the parameters, it is natural to ask whether the limiting procedures lead to the same physics. In particular, after taking the large-N limit, one may compare the limit in our setup with the $\mu \to 0$ limit of the supersymmetric deformation, and examine whether the resulting

dynamics and spacetime structure agree for the observables considered.

Acknowledgments

I would like to thank my supervisor Prof. Jun Nishimura for valuable discussions, advice, encouragement, and continuous support throughout this work.

I am also grateful to my collaborators, Prof. Asato Tsuchiya, Prof. Konstantinos N. Anagnostopoulos, Prof. Takahiro Azuma, Prof. Yuhma Asano, Dr. Stratos Kovalkov Papadoudis, Dr. Mitsuaki Hirasawa, Dr. Chien-Yu Chou, Dr. Ashutosh Tripathi, Mr. Worapat Piensuk, Mr. Cheng-Tsung Wang, and Mr. Tin Long Chau for fruitful discussions and collaborations.

Numerical simulations were carried out on Fugaku (Project IDs: hp250224 and hp240213), Grand Chariot at Hokkaido University (Project ID: hp240117), and Flow at Nagoya University (Project ID: hp250140).

A Lefschetz-thimble method

In this appendix we give a brief overview of the (generalized) Lefschetz-thimble method [22]. We first explain the sign problem and then show why a naive approach based on reweighting fails. Finally, we outline how the Lefschetz-thimble method resolves the sign problem.

A.1 The sign problem and reweighting

Let us consider a partition function of the form

$$Z = \int dx\, e^{-S(x)} \ . \tag{A.1}$$

The expectation value of an observable $\mathcal{O}$ is given by

$$\langle \mathcal{O}(x) \rangle = \frac{\int dx\, e^{-S(x)}\, \mathcal{O}(x)}{\int dx\, e^{-S(x)}} \ . \tag{A.2}$$

We assume $x \in \mathbb{R}^N$. When the action $S(x)$ is real, one can define the probability density

$$\rho(x) = \frac{e^{-S(x)}}{\int dx\, e^{-S(x)}} \tag{A.3}$$

and apply Monte Carlo methods.

If the action $S(x)$ is complex, however, $\rho(x)$ is no longer a positive real function and the probabilistic interpretation in Eq. (A.3) breaks down. As a result, standard Monte Carlo sampling cannot be used. A naive workaround is reweighting: writing $S(x) = \mathrm{Re}\, S(x) + i\, \mathrm{Im}\, S(x)$, one treats the real part $\mathrm{Re}\, S(x)$ as the sampling weight and includes the phase factor $e^{-i\, \mathrm{Im}\, S(x)}$ in the estimator:

$$\begin{aligned} \langle \mathcal{O}(x) \rangle &= \frac{\int dx\, e^{-\mathrm{Re}S(x) - i\mathrm{Im}S(x)}\, \mathcal{O}(x)}{\int dx\, e^{-\mathrm{Re}S(x) - i\mathrm{Im}S(x)}} \\ &= \frac{\left\langle e^{-i\mathrm{Im}S(x)} \mathcal{O}(x) \right\rangle_{\mathrm{rew}}}{\left\langle e^{-i\mathrm{Im}S(x)} \right\rangle_{\mathrm{rew}}} \ . \end{aligned} \tag{A.4}$$

Here $\langle \cdots \rangle_{\mathrm{rew}}$ denotes an expectation value computed with respect to the weight given only by the real part of the action,

$$\rho_{\mathrm{rew}}(x) = \frac{e^{-\mathrm{Re}S(x)}}{\int dx\, e^{-\mathrm{Re}S(x)}} \ . \tag{A.5}$$

Although reweighting appears to bypass the probabilistic issue, it fails in practice due to its computational cost. Because of the oscillatory factor $e^{-i\, \mathrm{Im}S(x)}$, severe cancellations occur

among configurations, making both the numerator and denominator extremely small:

$$\langle \mathcal{O}(x) \rangle = \frac{\left\langle e^{-i\mathrm{Im}S(x)} \mathcal{O}(x) \right\rangle_{\mathrm{rew}}}{\left\langle e^{-i\mathrm{Im}S(x)} \right\rangle_{\mathrm{rew}}} = \frac{e^{-O(N)}}{e^{-O(N)}} \ . \tag{A.6}$$

Since the statistical error of Monte Carlo estimates scales as $1/\sqrt{n}$ for n samples, one effectively has

$$\langle \mathcal{O}(x) \rangle = \frac{e^{-O(N)} \pm O(1/\sqrt{n})}{e^{-O(N)} \pm O(1/\sqrt{n})} \ . \tag{A.7}$$

Therefore, in order to obtain reliable results one needs $e^{-O(N)} \gg O(1/\sqrt{n})$, i.e., $n \gg e^{O(N)}$. In other words, the required number of samples grows exponentially with the system size. Hence, as N becomes large, obtaining accurate results by reweighting becomes practically impossible. This difficulty is the sign problem. It appears not only in the real-time evolution of quantum mechanics and IKKT matrix model as in this thesis, but also in finite-density QCD, real-time dynamics, and strongly correlated systems, among many other areas of theoretical physics.

A.2 Lefschetz-thimble method

We start from the same partition function and expectation value as in Eqs. (A.1) and (A.2):

$$Z = \int dx \, e^{-S(x)} \ , \tag{A.8}$$

$$\langle \mathcal{O}(x) \rangle = \frac{1}{Z} \int dx \, \mathcal{O}(x) \, e^{-S(x)} \ . \tag{A.9}$$

The Lefschetz-thimble method resolves the sign problem by deforming the integration manifold from the real domain $\mathbb{R}^N$ to an N-dimensional manifold embedded in the complexified space $\mathbb{C}^N$, using Cauchy's theorem and the (holomorphic) gradient flow [22]:

$$\frac{\partial}{\partial \sigma} z_k(x, \sigma) = \overline{\frac{\partial S\big(z(x,\sigma)\big)}{\partial z_k}} \ . \tag{A.10}$$

This equation is solved from the initial condition $z_k(x, 0) = x_k$ up to $\sigma = \tau$. The flowed configurations form the manifold

$$M_\tau \equiv \{ \, z(x, \tau) \mid x \in \mathbb{R}^N \, \} \subset \mathbb{C}^N. \tag{A.11}$$

By Cauchy's theorem, the integration contour can be deformed from $\mathbb{R}^N$ to M_τ without changing the value of the integral, provided no singularities are crossed. Since $z = z(x,\tau)$ gives a one-to-one map from $x \in \mathbb{R}^N$ to $z \in M_\tau$, the partition function can be written as

$$Z = \int_{M_\tau} dz\, e^{-S(z)}, \tag{A.12}$$

and similarly the expectation value in Eq. (A.9) becomes

$$\langle \mathcal{O}(x) \rangle = \frac{1}{Z} \int dz\, \mathcal{O}\big(z\big)\, e^{-S(z)}. \tag{A.13}$$

The key property of the flow (A.10) can be seen by evaluating the change of the action along the flow:

$$\begin{aligned} \frac{\partial}{\partial \sigma} S\big(z(x,\sigma)\big) &= \frac{\partial z_k(x,\sigma)}{\partial \sigma}\, \frac{\partial S\big(z(x,\sigma)\big)}{\partial z_k} \\ &= \overline{\frac{\partial S\big(z(x,\sigma)\big)}{\partial z_k}}\, \frac{\partial S\big(z(x,\sigma)\big)}{\partial z_k} \;\geq\; 0\,. \end{aligned} \tag{A.14}$$

Therefore the real part of the action increases monotonically along the flow, whereas the imaginary part is preserved:

$$\frac{\partial}{\partial \sigma} \operatorname{Re} S\big(z(x,\sigma)\big) \;\geq\; 0, \qquad \frac{\partial}{\partial \sigma} \operatorname{Im} S\big(z(x,\sigma)\big) \;=\; 0\,. \tag{A.15}$$

In the limit $\tau \to \infty$, configurations that do not flow into a critical point

$$\frac{\partial S(z^\star)}{\partial z_k} = 0 \tag{A.16}$$

are exponentially suppressed because $\operatorname{Re} S$ grows without bound along their flow lines. Hence the integral is dominated by neighborhoods of critical points and their associated thimbles, where $\operatorname{Im} S$ is approximately constant. This suppresses the rapid phase oscillations among configurations that cause severe cancellations in reweighting, thereby alleviating the sign problem.

More concretely, the failure of reweighting discussed in Eq. (A.4) originates from the fact that the average phase factor becomes exponentially small in the system size. After the contour deformation to M_τ, one may write the expectation value schematically as

$$\langle \mathcal{O} \rangle = \frac{\big\langle e^{i\varphi(z)}\, \mathcal{O}(z) \big\rangle_{M_\tau}}{\big\langle e^{i\varphi(z)} \big\rangle_{M_\tau}}\,, \tag{A.17}$$

where $\varphi(z)$ denotes the remaining complex phase on M_τ. Increasing τ suppresses phase fluctuations: for sufficiently large τ (in practice, chosen so that the residual sign problem

is mild), the magnitude of the average phase can remain of order $O(1)$, and one no longer needs an exponentially large number of samples to obtain reliable estimates.

At $\tau = \infty$, the manifold M_τ decomposes into the union of Lefschetz thimbles. When more than one thimble contributes, an ergodicity problem can arise for certain values of τ: the flow map cannot cross the zeros on M_τ, which can prevent transitions between thimbles and thus obstruct sampling of the correct equilibrium distribution. The generalized Lefschetz-thimble method (GTM) [23] avoids this issue by choosing τ to be sufficiently small that ergodicity is maintained, while still large enough that $\mathrm{Im}\, S\big(z(x,\tau)\big)$ does not exhibit violent oscillations. This approach is practically limited to relatively small system sizes, but it is useful for studies on the small system sizes. For example, in a bosonic model with $N = 2$, one can enumerate all saddle points and carry out the computation exhaustively by evaluating the contributions from the thimbles associated with each saddle [**?**]. For larger system sizes, avoiding the ergodicity problem generally requires integrating over τ [24].

B Derivation of the renormalized CM frequency in the molecular toy model

In this appendix we derive the renormalized center-of-mass (CM) frequency ω_r quoted in Sec. 4. We rewrite the constrained relative sector as a set of harmonic modes coupled linearly to the CM coordinate and determine the induced shift by completing the square. For later convenience, we also provide an equivalent expression that avoids diagonalizing the rank–1 deformed matrix and leads directly to the form used in the main text.

B.1 Starting point and reduction to one spatial component

We start from the Lagrangian (4.7). Since the three spatial components $\mu = 1, 2, 3$ are decoupled and identical in the present isotropic setup, it suffices to derive the result for a fixed μ and then restore μ at the end. This reduction simply exploits the spatial isotropy of the toy model: the μ components are identical and do not mix, so deriving the result for a fixed μ loses no information. For notational simplicity we suppress μ and write $X \equiv X_\mu$, $\xi^{(p)} \equiv \xi^{(p)}_\mu$. The μ-component Lagrangian reads

$$L = \frac{1}{2}\dot{X}^2 - \frac{c}{2N}X^2 + \frac{1}{2}\sum_{p=1}^{N}\Big(\dot{\xi}^{(p)}\Big)^2 - \frac{1}{2}\sum_{p,q=1}^{N}\xi^{(p)}H_{pq}\,\xi^{(q)} - \frac{c}{2}\big(\xi^{(N)}\big)^2 - \frac{c}{\sqrt{N}}\,X\,\xi^{(N)}, \quad \text{(B.1)}$$

subject to the constraint

$$\sum_{p=1}^{N} \xi^{(p)} = 0. \tag{B.2}$$

Here H_{pq} is the discrete Laplacian matrix introduced in the main text. The constraint removes the translational zero mode of the relative sector.

B.2 Constraint reduction and orthonormal coordinates

Introduce the N-component vector $\xi \equiv (\xi^{(1)}, \ldots, \xi^{(N)})^{\mathrm{T}} \in \mathbb{R}^N$. The constrained subspace (B.2) has dimension $N-1$. A convenient parametrization is obtained from the matrix

$$S = \big[e_1 - e_N,\ e_2 - e_N,\ \ldots,\ e_{N-1} - e_N\big] \in \mathbb{R}^{N\times(N-1)}, \tag{B.3}$$

where $\{e_p\}$ are the standard basis vectors of $\mathbb{R}^N$. Then any ξ satisfying $\sum_p \xi^{(p)} = 0$ can be written as $\xi = Sz$ with $z \in \mathbb{R}^{N-1}$.

Define

$$B \equiv S^{\mathrm{T}} S. \tag{B.4}$$

For the choice (B.3), one has explicitly

$$B_{ij} = (e_i - e_N)\cdot(e_j - e_N) = \delta_{ij} + 1 \qquad (i,j = 1,\ldots,N-1), \tag{B.5}$$

i.e. $B = I_{N-1} + \mathbf{1}\mathbf{1}^{\mathrm{T}}$ with $\mathbf{1} = (1,\ldots,1)^{\mathrm{T}}$. Diagonalize B as

$$B = Q\Lambda Q^{\mathrm{T}}, \qquad \Lambda = \mathrm{diag}(N, 1, \ldots, 1), \tag{B.6}$$

and define

$$U \equiv S\, Q\Lambda^{-1/2} \in \mathbb{R}^{N\times(N-1)}. \tag{B.7}$$

Then $U^{\mathrm{T}}U = I_{N-1}$, and any constrained ξ can be written as

$$\xi = U\, y, \qquad y \in \mathbb{R}^{N-1}. \tag{B.8}$$

Since U is orthonormal in the constrained subspace, the kinetic term becomes

$$\frac{1}{2}\sum_{p=1}^{N}\left(\dot{\xi}^{(p)}\right)^2 = \frac{1}{2}\,\dot{\xi}^{\mathrm{T}}\dot{\xi} = \frac{1}{2}\,\dot{y}^{\mathrm{T}}\dot{y}. \tag{B.9}$$

In these orthonormal coordinates, the kinetic term is invariant under $O(N-1)$ rotations $y \to Oy$. We will exploit this freedom to choose a basis in which the quadratic form of the relative sector is diagonal.

The Laplacian term reduces to a quadratic form in y:

$$\sum_{p,q=1}^{N} \xi^{(p)} H_{pq} \xi^{(q)} = y^{\mathrm{T}} \hat{H}\, y, \qquad \hat{H} \equiv U^{\mathrm{T}} H U \in \mathbb{R}^{(N-1)\times(N-1)}. \tag{B.10}$$

By construction, $\hat{H}$ is positive definite (the zero mode has been removed by the constraint).

B.3 Pinning vector and rank–1 deformation

Introduce the pinning vector $g \in \mathbb{R}^N$ selecting the distinguished site $p = N$,

$$g_p \equiv \delta_{p,N}. \tag{B.11}$$

Then $\xi^{(N)} = g^{\mathrm{T}}\xi$ and, using (B.8),

$$\xi^{(N)} = g^{\mathrm{T}} U\, y \equiv \beta^{\mathrm{T}} y, \qquad b \equiv U^{\mathrm{T}} g \in \mathbb{R}^{N-1}. \tag{B.12}$$

Substituting (B.8), (B.10), and (B.12) into (B.1), we obtain

$$L = \frac{1}{2}\dot{X}^2 - \frac{c}{2N} X^2 + \frac{1}{2}\,\dot{y}^{\mathrm{T}}\dot{y} - \frac{1}{2}\, y^{\mathrm{T}} \tilde{H}\, y - \frac{c}{\sqrt{N}}\, X\, b^{\mathrm{T}} y, \tag{B.13}$$

where the relative quadratic form is a rank–1 deformation

$$\tilde{H} \equiv \hat{H} + c\, b b^{\mathrm{T}}. \tag{B.14}$$

B.4 Normal modes and a CL-like form

Diagonalize $\tilde{H}$ by an orthogonal matrix $W \in SO(N-1)$,

$$\tilde{H} = W\, \mathrm{diag}(\omega_1^2, \ldots, \omega_{N-1}^2)\, W^{\mathrm{T}}. \tag{B.15}$$

The matrix $\tilde{H} = \hat{H} + c\, b b^{\mathrm{T}}$ is real and symmetric. Using the $O(N-1)$ freedom of the kinetic term, we rotate to the eigenbasis of $\tilde{H}$, i.e. we choose an orthogonal matrix W that diagonalizes $\tilde{H}$.

Define normal-mode coordinates q^k $(k = 1, \ldots, N-1)$ by

$$q \equiv (q^1, \ldots, q^{N-1})^{\mathrm{T}} \equiv W^{\mathrm{T}} y, \qquad y = W q, \tag{B.16}$$

and the projection coefficients

$$\tilde{\alpha} \equiv (\tilde{\alpha}_1, \ldots, \tilde{\alpha}_{N-1})^{\mathrm{T}} \equiv W^{\mathrm{T}} b, \qquad b^{\mathrm{T}} y = \tilde{\alpha}^{\mathrm{T}} q = \sum_{k=1}^{N-1} \tilde{\alpha}_k\, q^k. \tag{B.17}$$

Using (B.16)–(B.17), the Lagrangian (B.13) becomes

$$L = \frac{1}{2}\dot{X}^2 - \frac{c}{2N} X^2 + \sum_{k=1}^{N-1} \left[\frac{1}{2} \left(\dot{q}^k\right)^2 - \frac{1}{2}\omega_k^2 \left(q^k\right)^2 - \frac{c}{\sqrt{N}}\, \tilde{\alpha}_k\, X\, q^k \right]. \tag{B.18}$$

B.5 Completion of the square and the renormalized frequency

Complete the square for each mode q^k in (B.18):

$$-\frac{1}{2}\omega_k^2\left(q^k\right)^2-\frac{c}{\sqrt{N}}\,\tilde{\alpha}_k\,X\,q^k=-\frac{1}{2}\omega_k^2\left(q^k+\frac{c}{\sqrt{N}}\frac{\tilde{\alpha}_k}{\omega_k^2}X\right)^2+\frac{c^2}{2N}\frac{\tilde{\alpha}_k^2}{\omega_k^2}X^2. \tag{B.19}$$

Substituting this into (B.18), we obtain

$$L=\frac{1}{2}\dot{X}^2-\frac{1}{2}\omega_r^2X^2+\sum_{k=1}^{N-1}\left[\frac{1}{2}\left(\dot{q}^k\right)^2-\frac{1}{2}\omega_k^2\left(q^k+\frac{c}{\sqrt{N}}\frac{\tilde{\alpha}_k}{\omega_k^2}X\right)^2\right], \tag{B.20}$$

where the renormalized CM frequency is

$$\omega_r^2=\frac{c}{N}-\frac{c^2}{N}\sum_{k=1}^{N-1}\frac{\tilde{\alpha}_k^2}{\omega_k^2}=\frac{c}{N}-\frac{c^2}{N}\,b^{\mathrm{T}}\tilde{H}^{-1}b. \tag{B.21}$$

B.6 Equivalent expression via Sherman–Morrison and the main-text form

For later use it is convenient to rewrite (B.21) without diagonalizing $\tilde{H}=\hat{H}+c\,\beta\beta^{\mathrm{T}}$. Define

$$s_0\equiv b^{\mathrm{T}}\hat{H}^{-1}b,\qquad s(c)\equiv b^{\mathrm{T}}\tilde{H}^{-1}b. \tag{B.22}$$

Using the Sherman–Morrison formula for a rank–1 update, we obtain

$$(\hat{H}+c\,bb^{\mathrm{T}})^{-1}=\hat{H}^{-1}-\frac{c\,\hat{H}^{-1}bb^{\mathrm{T}}\hat{H}^{-1}}{1+c\,b^{\mathrm{T}}\hat{H}^{-1}b}, \tag{B.23}$$

and hence

$$s(c)=b^{\mathrm{T}}(\hat{H}+c\,bb^{\mathrm{T}})^{-1}b=\frac{s_0}{1+c\,s_0}. \tag{B.24}$$

Substituting (B.24) into (B.21), we find

$$\omega_r^2=\frac{c}{N}-\frac{c^2}{N}\frac{s_0}{1+c\,s_0}=\frac{c/N}{1+c\,s_0}. \tag{B.25}$$

This is the form quoted in the main text (Eq. (4.9)).

B.7 Restoring the spatial index

Finally, restoring the spatial index μ, the full Lagrangian is the sum $L=\sum_{\mu=1}^{3}L_\mu$, and the same ω_r is obtained for each component.

B.8 Comment on the correspondence with the Caldeira–Leggett notation

In Sec. 4 we keep the relative coordinates as $\xi_\mu^{(p)}$ with the site label p. Equation (B.16) shows that the normal modes q^k are obtained by an orthogonal change of variables within the constrained relative subspace. Therefore one may view the relative sector as an effective "bath" for the CM coordinate, with $\{\xi_\mu^{(p)}\}$ or equivalently $\{q^k\}$ playing the role of environment variables.

C Implementation of the "gauge-fixing"

We start from the gauge-fixed partition function(7.18)

$$Z_{\rm gf} = \int dA\; e^{iS[A]}\,\Delta_{\rm FP}[A]\,\prod_{i=1}^{9}\delta(\mathrm{tr}(A_0A_i))\ . \tag{C.1}$$

It is convenient to rewrite the Faddeev–Popov factor in the exponent as $\Delta_{\rm FP}[A] = \exp\big(\log\Delta_{\rm FP}[A]\big)$, so that

$$Z_{\rm gf} = \int dA\;\exp\Big(iS[A] + \log\Delta_{\rm FP}[A]\Big)\prod_{i=1}^{9}\delta(\mathrm{tr}(A_0A_i))\ . \tag{C.2}$$

For a stable numerical implementation, we introduce a sharply peaked term controlled by a real parameter $\alpha > 0$,

$$S_{\rm g.f.}^{(\alpha)} \equiv \frac{N}{2}\alpha\sum_{i=1}^{9}\Big(\mathrm{tr}(A_0A_i)\Big)^2\ . \tag{C.3}$$

We also represent the delta-function constraints by auxiliary variables k^i through a Fourier representation (overall constants are omitted),

$$\prod_{i=1}^{9}\delta(\mathrm{tr}(A_0A_i))\ \propto\ \int dk\;\exp\left(iN\kappa\sum_{i=1}^{9}k^i\,\mathrm{tr}(A_0A_i)\right),\qquad dk\equiv\prod_{i=1}^{9}dk^i\ , \tag{C.4}$$

where κ is a real parameter controlling the sharpness of the constraint. Correspondingly, we define

$$S_{\rm g.f.}^{(k)} \equiv -iN\kappa\sum_{i=1}^{9}k^i\,\mathrm{tr}(A_0A_i)\ . \tag{C.5}$$

With these ingredients, we define the effective partition function used in simulations as

$$Z_{\rm eff} \equiv \int dA\,dk\;e^{-S_{\rm eff}[A,k]}\ . \tag{C.6}$$

Here the effective action is

$$S_{\text{eff}}[A,k] = -iS[A] + S_{\text{g.f.}}[A,k] \ , \tag{C.7}$$

with the gauge-fixing contribution

$$S_{\text{g.f.}}[A,k] \equiv -\log \Delta_{\text{FP}}[A] + S^{(\alpha)}_{\text{g.f.}} + S^{(k)}_{\text{g.f.}} \ . \tag{C.8}$$

In the limits $\alpha \to \infty$ and/or $\kappa \to \infty$, these terms enforce $\mathrm{tr}(A_0 A_i) = 0$ sharply, reproducing the delta-function constraints in (C.1). In practice, α and κ are chosen sufficiently large so that $\mathrm{tr}(A_0 A_i)$ is driven to zero within statistical errors in simulations.

D Supersymmetric deformation

In this appendix, we discuss the connection between the model studied in this work and a class of supersymmetry-preserving deformations of the type IIB matrix model [25]. Specifically, we consider a deformed model S' of the original action S:

$$S' = S + S_\gamma + S_{\text{Myers}} + S_{m_{\text{f}}} \ , \tag{D.1}$$

where S is defined in Eq. (6.1). The terms S_γ and $S_{m_{\text{f}}}$ are given by Eqs. (9.3) and (9.2), respectively:

$$\begin{aligned} S_\gamma &= \frac{1}{2} N\gamma \left(\mathrm{tr}\,(A_0)^2 - \sum_{i=1}^{\tilde{d}} \mathrm{tr}\,(A_i)^2 - \xi \sum_{j=\tilde{d}+1}^{9} \mathrm{tr}\,(A_j)^2 \right) \ , \\ S_{m_{\text{f}}} &= -\frac{N}{2}\, i m_{\text{f}}\, \mathrm{tr} \bar{\Psi} (\Gamma^7 (\Gamma^8)^\dagger \Gamma^9) \Psi \ . \end{aligned}$$

In addition, S_{Myers} is the so-called Myers term,

$$S_{\text{Myers}} = -iN\zeta \mathrm{Tr}\,(A_7 [A_8, A_9]) \ , \tag{D.2}$$

which introduces cubic interactions among three specific spatial directions.

By choosing the deformation parameters as

$$\tilde{d} = 6 \ , \quad \gamma = -\frac{\mu^2}{32} \ , \quad \xi = 3 \ , \quad \zeta = \mu \ , \quad m_{\text{f}} = \frac{\mu}{4} \ , \tag{D.3}$$

with a real parameter μ, the full action S' becomes invariant under a deformed supersymmetry transformation:

$$\begin{aligned} \delta A_\mu &= i\bar{\epsilon}\Gamma_\mu \psi \ , \\ \delta \Psi &= \frac{i}{2}[A_\mu, A_\nu]\Gamma^{\mu\nu}\epsilon + \frac{\mu}{8}((\Gamma^\mu)^\dagger \Gamma^7 (\Gamma^8)^\dagger \Gamma^9 + 2(\Gamma^7)^\dagger \Gamma^8 (\Gamma^9)^\dagger \Gamma^\mu) A_\mu \epsilon \ , \end{aligned} \tag{D.4}$$

where ϵ is a constant Majorana-Weyl spinor in $(9+1)$ dimensions, and $\Gamma^{\mu\nu} = -((\Gamma^{\mu})^{\dagger}\Gamma^{\nu} - (\Gamma^{\nu})^{\dagger}\Gamma^{\mu})/2$.

We emphasize that this deformation preserves 16 supercharges out of the original 32 of the type IIB matrix model. The structure of the bosonic and fermionic mass terms, along with the Myers term, plays a crucial role in realizing this partial SUSY preservation.

In contrast, the model studied in this work (Sec. 9.2) corresponds to S' with $\tilde{d} = 5$, $\zeta = 0$, and $(\gamma, \xi, m_{\mathrm{f}})$ being real positive constants. While this breaks all SUSY, the deformation retains the same functional form and can be viewed as a generalization of the above supersymmetric deformation, adapted for the purpose of enhancing the effectiveness and stability of complex Langevin simulations.

References

[1] A. O. Caldeira and A. J. Leggett, *Path integral approach to quantum Brownian motion*, *Physica A* **121** (1983) 587.

[2] A. O. Caldeira and A. J. Leggett, *Quantum tunneling in a dissipative system*, *Annals Phys.* **149** (1983) 374.

[3] W. G. Unruh and W. H. Zurek, *Reduction of a wave packet in quantum Brownian motion*, *Phys. Rev. D* **40** (1989) 1071.

[4] J. Nishimura and H. Watanabe, *Quantum decoherence in the Caldeira-Leggett model by the real-time path integral on a computer*, *JHEP* **09** (2025) 197 [2503.20699].

[5] R. P. Feynman and F. L. Vernon, Jr., *The theory of a general quantum system interacting with a linear dissipative system*, *Annals Phys.* **24** (1963) 118.

[6] N. Ishibashi, H. Kawai, Y. Kitazawa and A. Tsuchiya, *A large N reduced model as superstring*, *Nucl. Phys. B* **498** (1997) 467 [hep-th/9612115].

[7] J. Nishimura and A. Tsuchiya, *Complex Langevin analysis of the space-time structure in the Lorentzian type IIB matrix model*, *JHEP* **06** (2019) 077 [1904.05919].

[8] K. Hatakeyama, K. Anagnostopoulos, T. Azuma, M. Hirasawa, Y. Ito, J. Nishimura et al., *Complex Langevin studies of the emergent space-time in the type IIB matrix model*, in *Proceedings of the East Asia Joint Symposium on Fields and Strings 2021*, 2201.13200.

[9] J. Nishimura, *Signature change of the emergent space-time in the IKKT matrix model*, *PoS* **CORFU2021** (2022) 255 [2205.04726].

[10] M. Hirasawa, K. N. Anagnostopoulos, T. Azuma, K. Hatakeyama, J. Nishimura, S. K. Papadoudis et al., *The emergence of expanding space-time in a novel large-N limit of the Lorentzian type IIB matrix model*, *PoS* **LATTICE2022** (2023) 371 [2212.10127].

[11] H. C. Steinacker, *Cosmological space-times with resolved Big Bang in Yang-Mills matrix models*, *JHEP* **02** (2018) 033 [1709.10480].

[12] Y. Asano, J. Nishimura, W. Piensuk and N. Yamamori, *Defining the Type IIB Matrix Model without Breaking Lorentz Symmetry*, *Phys. Rev. Lett.* **134** (2025) 041603 [2404.14045].

[13] T. Aoki, M. Hirasawa, Y. Ito, J. Nishimura and A. Tsuchiya, *On the structure of the emergent 3d expanding space in the Lorentzian type IIB matrix model*, *PTEP* **2019** (2019) 093B03 [1904.05914].

[14] G. Parisi, *ON COMPLEX PROBABILITIES*, *Phys. Lett. B* **131** (1983) 393.

[15] J. R. Klauder, *Coherent state Langevin equations for canonical quantum systems with applications to the quantized Hall effect*, *Phys. Rev.* **A29** (1984) 2036.

[16] J. Nishimura and A. Tsuchiya, *Complex Langevin analysis of the space-time structure in the Lorentzian type IIB matrix model*, *JHEP* **06** (2019) 077 [1904.05919].

[17] J. Nishimura and S. Shimasaki, *New Insights into the Problem with a Singular Drift Term in the Complex Langevin Method*, *Phys. Rev. D* **92** (2015) 011501 [1504.08359].

[18] K. Nagata, J. Nishimura and S. Shimasaki, *Argument for justification of the complex Langevin method and the condition for correct convergence*, *Phys. Rev. D* **94** (2016) 114515 [1606.07627].

[19] G. Aarts, E. Seiler and I.-O. Stamatescu, *The Complex Langevin method: When can it be trusted?*, *Phys. Rev. D* **81** (2010) 054508 [0912.3360].

[20] J. Nishimura and S. Shimasaki, *New insights into the problem with a singular drift term in the complex Langevin method*, *Phys. Rev.* **D92** (2015) 011501 [1504.08359].

[21] K. Nagata, J. Nishimura and S. Shimasaki, *Argument for justification of the complex Langevin method and the condition for correct convergence*, *Phys. Rev.* **D94** (2016) 114515 [1606.07627].

[22] A. Alexandru, G. Basar, P. F. Bedaque, G. W. Ridgway and N. C. Warrington, *Sign problem and Monte Carlo calculations beyond Lefschetz thimbles*, *JHEP* **05** (2016) 053 [1512.08764].

[23] A. Alexandru, G. Basar, P. F. Bedaque and N. C. Warrington, *Complex Paths Around The Sign Problem*, 2007.05436.

[24] M. Fukuma and N. Matsumoto, *Worldvolume approach to the tempered Lefschetz thimble method*, *PTEP* **2021** (2021) 023B08 [2012.08468].

[25] G. Bonelli, *Matrix strings in pp wave backgrounds from deformed super Yang-Mills theory*, *JHEP* **08** (2002) 022 [hep-th/0205213].